**UNIVERSIDAD AUTÓNOMA DE NUEVO LEÓN**

**FACULTAD DE CIENCIAS QUÍMICAS**

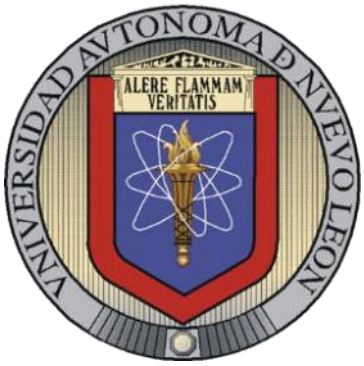


**TESIS**

# DEVELOPMENT OF POLYTHIOPHENE FILMS WITH GRAPHENE FOR ITS APPLICATION IN FLEXIBLE ELECTRONICS

**PRESENTADA POR**

**M.C. JOSÉ MANUEL MARTÍNEZ PÉREZ**

**COMO REQUISITO PARCIAL PARA OBTENER EL GRADO DE**
**DOCTORADO EN CIENCIAS**
**CON ORIENTACIÓN EN QUÍMICA DE LOS MATERIALES**

**AGOSTO, 2024**

**“DEVELOPMENT OF POLYTHIOPHENE FILMS WITH GRAPHENE FOR ITS APPLICATION IN FLEXIBLE ELECTRONICS”**

**Aprobación de la Tesis:**

_____

**M.C. José Manuel Martínez Pérez**

**Proponente**

_____

**Dra. Ma. Idalia Gómez de la Fuente**

**Directora de Tesis**

**San Nicolás de los Garza, Nuevo León a Septiembre del 2023**

**“DEVELOPMENT OF POLYTHIPHENE FILMS WITH GRAPHENE FOR ITS APPLICATION IN FLEXIBLE ELECTRONICS”**

**Revisión de la Tesis:**

_____

**M.C. José Manuel Martínez Pérez**

**Proponente**

_____

**Dra. Ma. Idalia Gómez de la Fuente**

**Directora de Tesis**

**San Nicolás de los Garza, Nuevo León a Septiembre del 2023**

# RESUMEN

José Manuel Martínez Pérez  Fecha de Graduación: Diciembre,2023

Universidad Autónoma de Nuevo León

Facultad de Ciencias Químicas

Título del Estudio: **"DEVELOPMENT OF POLYTHIOPHENE FILMS WITH GRAPHENE FOR ITS APPLICATION IN FLEXIBLE ELECTRONICS"**

**Numero de Paginas:** **Candidato para el grado de Doctorado en Ciencias con Orientación en Química de Materiales**

**Área de Estudio: Materiales para Electrónica Flexible**

**Propósito y Método del estudio:** Los compuestos de politiofeno están siendo ampliamente investigados para su uso en dispositivos electrónicos como celdas solares híbridas, y más. El interés en estos compuestos se basa en su conductividad eléctrica, propiedades ópticas, estabilidad térmica y química, y la capacidad para crear dispositivos flexibles. El grafeno por su parte posee propiedades eléctricas que lo convierten en un material de gran interés para la fabricación de circuitos electrónicos en los cuales se integrara con a una matriz polimérica y serán aprovechados para dicho fin.

**Contribuciones y Conclusiones:** La fabricación de circuitos con biocompatibilidad y potencial aplicación en diferentes ámbitos como la medicina, los robots suaves, circuitos flexibles, reducción de peso en circuitos, mejora de propiedades térmicas y mecánicas, etc.

## FIRMA DEL ASESOR:

# Index

## ABBREVIATIONS

| | |
|---|---|
| AuNPs | Gold nanoparticles |
| CVD | Chemical Vapor Deposition |
| DLS | Dynamic light scattering |
| EDS | X-ray Energy Dispersion Spectrometry |
| FCC | Cubic Structure Centered on the faces |
| FESEM | Field emission Scanning Electronic Microscopy |
| FTIR | Fourier Tranform Infrarred Spectroscopy |
| GO | Graphene Oxide |
| GQD | Graphene Quantum Dots |
| ITO | Indium-tin oxide |
| PSC | Photovoltaic solar cells |
| PTh | Polythiophene |
| rGO r | Reduced graphene oxide |
| SEM | Scanning Electronic Microscopy |
| TEM | Transmission Electronic Microscopy |
| XRD | X-ray Diffraction |

# 1. INTRODUCTION

Highly conductive films are extremely attractive for a range of electronic devices, particularly printed macroelectronics. For example, the replacement of heavy-metal current collectors with thin, light, flexible, and highly conductive films will further improve the energy density of such devices. Films with two-dimensional building blocks, such as graphene or reduced graphene oxide (rGO), are particularly promising because of their low percolation thresholds with a high aspect ratio, excellent flexibility, and low cost. However, the electrical conductivity of these films is low [1].

In order to improve the different characteristics of the materials you can find reports have been published on different types of nanoparticle decorations where the size and shape of the particles influence the performance of the compound, for example, graphene oxide particles printed materials where the size of chemically modified graphene nanolines is a critical parameter that affects their performance and applications[2]. On the other hand, graphene nanosheets obtained through the process of oxidation and exfoliation of graphite have attracted much interest in the field of colloidal sciences and with respect to technical applications in printed electronics [3–5].

Reduced graphene oxide nanosheets (rGO) are very attractive due to their large lateral size (up to hundreds of micrometers) after processing, which results in a much lower percolation threshold and fewer joints in a continuous film, causing properties of high electrical conductivity [1].

The development of graphene in flexible and stretchable electronics has recently attracted attention, and this has led to a series of new applications, such as circuit printing [3], cybernetic skin[6],portable devices[7,8] y biosensors[9]. Although the flexibility of graphene-based materials makes them the ideal candidate as an electrically conductive component, the introduction of nanomaterials also allows its use in new approaches for the construction of electrochemical biosensors. [2,10,11].

In the case of photovoltaic solar cells (PSC) these are typically manufactured on substrates coated with transparent indium oxide and tin oxide (ITO) electrodes, which represents an obstacle to the successful commercialization of PSCs. In fact, the ITO is not an ideal material due to its high cost and mechanical flexibility [11].

## 1.1. FLEXIBLE ELECTRONICS

Nanotechnology has been widely studied and used in many fields, such as electronics, photonics, materials science, chemistry, biology, and medicine. In the fields of biomedicine and multidisciplinary biophotonics, nanomaterials are used for drug administration, therapy, detection, and imaging. At present, the use of carbonate-based materials, particularly graphene quantum dots (GQD), as contrast agents has attracted considerable attention. Quantum dots are nanoparticles with size-dependent optical properties and electrons and offer promising advantages such as fluorescence and high photostability in biological applications; in addition, numerous applications have been proposed in fields such as photovoltaic devices, lighting-saving screens, and biomarkers [12].

For its part, the development of technology in the field of flexible electronics has quite a history, around the decade of the 70's the crystalline silicon solar cells were thinned to increase their power / weight ratio for use in satellites. This is because the cells were thin and flexible. In today's applications, silicon-based integrated circuits are thin and sturdy; for example, a card is not damaged when accidentally sitting on it. Flexible can mean many qualities, such as elasticity, light weighted, and tenacity. [13].

There are two basic approaches to manufacturing these flexible electronic devices: (1) transfer and joining of circuits assembled on a flexible substrate, and (2) fabrication of circuits directly on flexible substrates.

Efforts are currently being made to develop a new class of fully biodegradable "green" compounds by combining fibers (bio / natural) with biodegradable resins [14]. The main attraction of green compounds is that they are respectful with the environment, totally degradable and sustainable, that is, they are truly "green" in every way.

These green compounds can be effectively used in many applications, such as mass-produced consumer products with relatively short life cycles of one–two years (non-durable) or products intended for one-time or short-term use (seldom) before elimination [14].

Sustainable organic eco-products are products with commercial and environmental acceptability derived from renewable resources, with recycling capacities and/or unleashed biodegradability [15]. As a result of new legislation on the development of ecologically and economically viable manufacturing, as well as the reuse and recycling of materials [16], the market for biopolymers and biocomposites is growing rapidly.

This type of technology can be used to develop different types of devices such as flexible screens, touch panels, etc.[4,8] The biggest advantage of these materials is that they can undergo large plastic deformation without causing any damage to unprotected devices.

## 1.2. POLYTHIOPHENE FILMS

Polythiophene is a type of conjugated polymer with properties that make it suitable for various applications, such as materials for thin films, and different techniques may be used to synthesize these films because polythiophene molecules can be deposited onto a substrate via spin coating, dip-coating, vapor deposition, and electrochemical cells. Depending on the final necessary characteristics, different variables may be tinkered with to get what you may need.

Conductive polymers like polythiophene (PTh) have unique properties such as environmental stability, good electrical conductivity, and other special properties, making them good candidates for the development of flexible electronic components since it can be dispersed into other liquids and be deposited in layers as a protective coating.[17]

Polythiophene composites are being extensively researched for use in electronic devices such as hybrid solar cells, light-emitting diodes, hydrogen storage, batteries, electrochromic devices, biosensors, and more [18–21]. The interest in these composites is based on their electrical conductivity, optical properties, thermal and chemical stability, and the ability to create flexible devices. Polythiophene and its composites can be successfully fabricated by chemical or electrochemical polymerization and exhibit various electrical and optical properties. An important feature of the electrochemical process is the possibility of growing thin films with high homogeneity.

Highly conductive films hold immense appeal across a wide spectrum of electronic devices, with a particular focus on their application in printed macroelectronics. The potential to replace conventional heavy, metal-based current collectors with thin, lightweight, and remarkably conductive films promises to yield significant enhancements in the energy density of these devices. One of the candidates stands out in this kind of is films composed of two-dimensional building blocks, notably graphene or nanosheets of reduced graphene oxide (rGO). [22]

It's important to remember that graphene and rGO-based films are enhancing electronic device performance in a substantial manner, but their full potential in flexible optoelectronic devices and solar cells is still an area of active research and exploration.

## 1.3. GRAPHENE

First isolated in 2004, graphene is a two-dimensional allotrope of carbon that has gained much attention in the scientific community in recent years because of its excellent mechanical, electrical, and optical properties, making it an excellent candidate for applications in electronics, electronic devices, collections, sensors, biological-inspired devices, and other systems [7,23]. Graphene is an allotropic form of graphite, a material that consists of two dimensions on a flat surface of hexagonal structure and has only one atom of C in thickness, on the other hand,

there are other allotropic forms such as fullerenes (ellipsoids or hollow spheres) and the carbon nanotubes (cylindrical) which are three-dimensional structures that are structures formed from a sheet of graphene as seen in Figure 1. Graphene, being a newly discovered material, the investigations carried out with respect to said material show that it has excellent electrical, magnetic, and mechanical properties as well as a high specific surface[24].

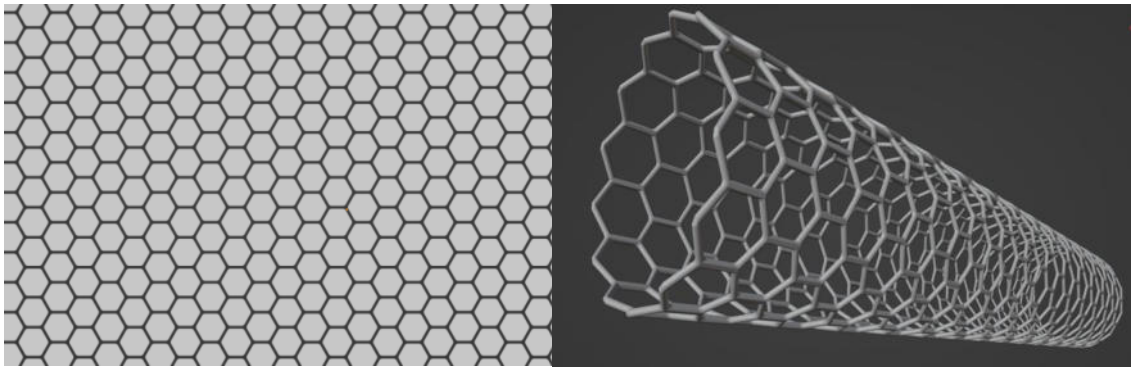

*Figure 1.- Graphene lattice as the basis for other carbon allotropes like carbon nanotubes.*

During the past few years, various procedures have been established to produce graphene, such as mechanical or ultrasonic exfoliation,[7,23,25] chemical vapor deposition [26], epitaxial growth [27], and chemical routes via the reduction of graphene oxide.

Starting with the top-down physical methods, mechanical exfoliation is a physical method for obtaining graphene by separating the graphite by using adhesive tape to separate its layers, the next step after making the separation, the procedure

continues with dissolving the medium adhesive used to obtain only the graphene sheets. On the other hand, in the ultrasonic method, ultrasound is used to carry out the exfoliation of the graphite layers and can be assisted by solvents and/or surfactants that help the dispersion of the particles; however, these aforementioned methods are methods which do not require specialized equipment but as a disadvantage, a very wide dispersion of particle-size is obtained, this affects negatively since to have some particular properties of graphene (mainly mechanical properties) a relatively low particle size dispersion is required [7].

The top-down chemical method involves the oxidation of graphite, which, when incorporating other functional groups, weakens the structure and allows the separation of the graphene oxide layers, which undergo a reduction process to obtain graphite layers without adhered functional groups [28,29].

Continuing with chemical methods, bottom-up procedures such as epitaxial molecular beam growth (also known as molecular beam epitaxy) and chemical vapor deposition (CVD), chemically pure growth of graphene can be obtained on a substrate, providing this advantage over the control of the properties and the quality of the product of the synthesis; however, the disadvantages of these methods are that they have a much higher cost than chemical synthesis methods and require specialized equipment to obtain them [4,26,27].

Graphene has been the focus of extensive research owing to its excellent physical properties [3,4,7,8,12,28,30–41]. It has an excellent thermal conductivity of

approximately 5000 W/mK [30], which is an order of magnitude higher than that of Cu. Graphene also has a very high theoretical surface area of ~ 2600 $m^2$ / g, [42] and a relatively low density of 2.2 g / $cm^3$, compared to conductive metals such as copper (density = 8.96 g / $cm^3$). The graphene tensile modulus of ~ 1 TPa is significantly higher than the steel value of ~ 200 GPa. Finally, graphene has an electronic mobility of 2.5 * $10^5$ $cm^2$ / Vs, compared to silicon's value of 1400 $cm^2$ / Vs and the value of carbon nanotubes of 1 * $10^5$ $cm^2$ / Vs[37].

# 2. BACKGROUND

The research carried out by the research group of Mohanty et. al. consisted in the analysis of plastic composite materials reinforced with natural fibers, providing information on the properties of biofibers, degradation processes, as well as the cost of production and sustainable development of them. In biocomposites, biofibers serve as reinforcement by increasing the strength and rigidity of the resulting composite structures [43]. In a previous work, it was mentioned that the properties also depend on where the biofibers are obtained, since they are different if they are obtained from the leaves or roots of a plant [44].

Netravali et al. reported that research efforts are currently focusing on the development of a new class of "totally green" compounds, which are completely biodegradable, combining fibers (natural/biofibers) with biodegradable resins. The main reasons to be concerned with the development of green composite materials are that they are environmentally friendly, totally biodegradable, and sustainable, that is, they are truly "green" in all respects, which would reduce the use of non-recyclable materials in single-use or short-life devices; consequently, this would contribute to the reduction of electronic waste [14].

John et al. They carried out an analysis on biofibers and biocomposites in which they mentioned their advantages and disadvantages. The recent and growing interest in lignocellulosic fibers is since the production of these fibers is cheap with few equipment needs; they present low specific weight, greater specific

resistance, and rigidity compared to materials made with reinforced glass. Moreover, these biofibers are not abrasive for mixing and molding, which can contribute to the reduction of costs in terms of equipment maintenance [45].

In 2007, Park et al. investigated the control over the size of the Cu nanoparticles during the synthesis and found that the particles obtained were crystallized copper with a cubic structure centered on the faces (FCC), with a spherical morphology of 45 ± 8 nm in diameter. The size of the spheres and their distribution were controlled by varying the synthesis parameters, such as the concentration of the reducing agent, reaction temperature, and injection rate of the precursor. In addition, it was also observed that the particle size distribution was less dispersed when the lowest temperature used for its synthesis was 140 °C [46].

By contrast, Soroudi et al. They conducted research on recycling multiple types of biomaterials. In recent years, the recycling of polymers and their mixtures has been studied using mechanical and chemical methods, whereas in biocomposites, research has focused on mechanical recycling. As defined by Mohanty et al., biocomposites are composite materials in which at least one component is derived from natural resources [47]. A sustainable biocomposite must satisfy several requirements.

1. It is made from renewable resources and/or recycled resources.
2. The synthesis and/or modification operations must be performed under favorable and effective energy mechanisms.

3. All stages of its life cycle must be free of hazardous or toxicological environmental impacts.
4. They applied waste-management options [48].

It is important that all biocomposites are susceptible to abiotic degradation processes; that is, they are not broken down by other physical and/or chemical processes. The absorption of water and biodegradation must be considered in the design, thus ensuring its structural and functional stability during its useful life. Therefore, biocomposites cannot easily be called sustainable materials [49].

In relation to graphene, a single sheet of graphite, which has electrical, thermal, mechanical, and special properties derived from its unique structure [7,8,31–33,35], can be found, and the work of Eda et al., where the properties of graphene are discussed for use in compounds applied in the field of electronics; when they are incorporated into polymer or ceramic matrices, the authors mention that their properties manifest themselves with significant improvements in the host material. Compounds based on polymers and graphene exhibit an extremely low electrical threshold percolation owing to the high proportion of conductivity and appearance of graphene sheets (atomic thickness and lateral dimensions of micro size) [32]. The graphene used in this study was synthesized using the method described by Stankovich et al., which was prepared by treating graphite oxide (GO) with organic isocyanates. The isocyanate graphene oxides were subsequently exfoliated into functionalized graphene oxide nanoplatelets, which can form a stable dispersion in polar aprotic solvents [50].

Kuo et al. conducted research on polymers conjugated with GQD and reported that there is a dependence on the optical properties and electrons of these particles related to their size, as well as advantages such as fluorescence and high photostability in biological applications. They used techniques such as SEM and TEM to analyze the characteristics of these particles that were prepared from a chemical method by oxidation of graphite obtaining sizes of 1.05 ± 0.2 nm, which is slightly above the thickness reported for the graphene, which is approximately 0.36 nm, indicating that this was due to the adhesion of functional groups on the surface of the oxide [12].

# 3. CRITICAL ANALYSIS

In the reviewed works, it was found that several research groups have developed composites with polymers, and some report a mixture with biopolymers; however, none of them reported the use of a biopolymer with graphene decorated with gold. Therefore, we wanted to test the realization of a synthesis of a biocomposite because, although there is much work done with these substances, the use of sodium alginate has not been reported as a component to form a conductive biofilm that could have a bioapplication/biointegration, with the purpose of manufacturing graphene biofilm devices containing gold in its conformation. This, with the objective of testing the effect and studying the "exciton-plasmon" phenomenon, for its application in optoelectronic devices.

Previously, it has been reported that the mechanical and thermal properties of sodium alginate are not optimal because of their low thermal stability and poor mechanical properties[51], but for this it is intended to synthesize graphene with the favorable properties that are required and with this when forming the biocomposite; the disadvantages of alginate are counteracted using the advantages of graphene[52], causing a synergy of properties. This provides an immediate response to the requirement of new legislation on the development and manufacturing of ecologically and economically viable materials, as well as the reuse and recycling of materials with applications in electronics and optoelectronics [16].

# 4. HYPOTHESIS

The electrical synergies between graphene and polythiophene are expected to enhance the conductivity and optical characteristics of the resulting hybrid films.

# 5. OBJECTIVES AND GOALS

## 5.1. GENERAL OBJECTIVE

Utilize electrochemical synthesis with voltamperometric techniques to fabricate hybrid films comprising reduced graphene oxide and polythiophene, aiming to enhance both photonic and conductive properties.

## 5.2. SPECIFIC OBJECTIVES

- Synthesis of reduced graphene sheets by the chemical hummers method of graphite oxidation assisted with ultrasound bath.

- Characterize graphene particles and films with X-ray diffraction (XRD), Fourier Transform Infrared spectroscopy (FTIR), Field Emission Scanning Electronic Microscopy with Energy Dispersive X-ray Spectroscopy (FESEM-EDX) and Transmission Electronic Microscopy (TEM).

- Synthesize films with reduced graphene oxide and polythiophene using potentiostat/galvanostat electrochemical methods.

- Conductivity tests were conducted using electrochemical impedance spectroscopy with a potentiostat/galvanostat.

# 6. METHODOLOGY

This section provides an in-depth account of the carefully crafted experimental procedure that underpins the development of this project. The process unfolds in several stages, each contributing to the realization of a flexible polymer film with enhanced electronic properties, achieved through the strategic incorporation and electrochemical reduction of graphene oxide (GO).

## 6.1. GRAPHENE OXIDE SYNTHESIS

At present, the chemical conversion of graphite into graphene oxide (GO) has turned out to be a viable route to produce individual sheets based on graphene in considerable quantities. Graphene oxide is generally synthesized through the oxidation of graphite using oxidizers, including concentrated sulfuric acid, nitric acid, and potassium permanganate, based on the Hummers method [3,8,12,28,35,40,52,53].

In comparison with pure graphite, GO is strongly oxygenated with hydroxyl and epoxy groups on $sp^3$ hybridized carbon in the basal plane, in addition to carbonyl and carboxyl groups located at the edges of the $sp^2$-hybridized carbon sheet. Therefore, GO is highly hydrophilic and easily exfoliated in water, providing a stable dispersion consisting mainly of single-layer sheets (graphene oxide)[54].

The synthesis was carried out as follows. In a round-bottomed flask, graphite powder was placed in an acidic medium, placed in an ice bath, and then an oxidizing agent was added. In our case, potassium permanganate ($KMnO_4$) was stirred for 30 min and continued stirring for another 2 h at a temperature of 35 °C. Distilled water was added, while maintaining a temperature of approximately 100 °C for 15 min. Next, a 30% hydrogen peroxide solution was added, and the product was filtered with a 10% hydrochloric acid (HCl) solution. The samples were thoroughly washed with distilled water to remove remnants of the synthesis as well as an acid wash [52,55].

The acid wash was performed using 50 ml centrifuge tubes at 4000 RPM on 5 minutes periods, first remaining solution gets mixed to make it as homogenic as possible separating it into the available tubes, after being centrifuged solids remain at the bottom of the tube and liquids are decantated, the acid is added to the remaining solids and the tube gets vigorously agitated to ensure proper contact between the acid solution and the prepared GO, this process is repeated until all the prepared acid is used.

After the acid wash is finished a water wash is also needed to wash the GO, so the process is basically the same as the acid wash but using distilled water, pH is also monitored until reaching a pH close to 7 being measured with pH strips.

Afterwards a solution with the remaining solids using 250 ml of distilled water to keep GO suspended (around 1 ml per mg of GO), then the solution remained

goes into an ultrasonic bath for 1 hour to help separate the obtained layers of GO before being dried out for storage.

The drying process of the GO obtained was performed in an oven operating at 60 °C for 8 hours in a petri dish, the final product is later pulverized for easier handling and storage.

## 6.1. POLYTHIOPHENE FILMS ELECTROCHEMICAL SYNTHESIS

The polymers and composites used in this study were synthesized using electrochemical methods. Parameters such as the voltage, current density, time, electropolymerization method, monomer concentration, type of electrolyte, and type of solvent control the electropolymerization process. To achieve this, an PGSTAT302N Metrohm AutoLab Potentiostat/Galvanostat was used. In the case of the polythiophene synthesis, the method used was cyclic voltammetry to get to know in the first place the properties of the polymer formation and behavior by looking at the potentials of the anodic and cathodic peaks corresponding to processes of oxidation and reduction, respectively.

All experiments were performed at room temperature using a three-electrode electrochemical cell with ITO glass as the working electrode, a platinum wire as the counter electrode, and saturated Ag/AgCl as the reference electrode. PTh thin films were obtained from a solution containing 0.5 M thiophene monomer and

0.1 M tetrabutylammonium hexafluorophosphate ($Bu_4NPF_6$) in dried acetonitrile with a fixed potential of 1.9 V vs Ag/AgCl.

### 6.1.1. POLYTHIOPHENE FILMS SYNTHESIS USING CYCLIC VOLTAMMETRY

The films were synthesized by preparing 100mL of solution with the thiophene monomer (0.5 M) and the support electrolyte, which in this case was tetrabutylammonium hexafluorophosphate ($Bu_4NPF_6$), dissolved in dehydrated acetonitrile.

Afterward, the solution was poured into a beaker to prepare the electrochemical cell and the method used was cyclic voltammetry (CV) (Figure 2) to scan and study the behavior of the polymer formation process in order of the oxidation and reduction processes taking place (Figure 2), this was performed for 5 cycles at different scan rate speeds (5,15,25,50,100 mV/s), the working electrode was an ITO covered substrate, a platinum counter electrode and an electrode made of Silver/Silver Chloride (Ag-AgCl) as the reference electrode.

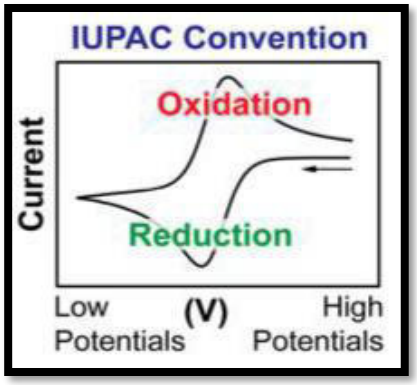


*Figure 2 IUPAC Convention for data reporting in cyclic voltammetry* [56]

Different combinations of parameters and working electrode types make for a long list of techniques, including voltammetry, polarography, cyclic voltammetry, linear sweep techniques, chronoamperometry, chronopotentiometry, and pulsed techniques [57].Cyclic voltammetry was the method used to obtain the polymer film which is carried out by doing potential sweeps on a determined potential window which in this case was from -0.6 to 2.0V, the advantage of this method is that we can keep on monitoring the events that happen and the electrochemical characteristics of the growth during polymerization. The electropolymerization process of the polythiophene film consists of the monomer being first oxidized by the application of the corresponding oxidation potential, which favors the formation of monomer cations that concentrate on the working electrode surface and form a thin film.

### 6.1.2. POLYTHIOPHENE FILM SYNTHESIS

The electrochemical method employed for the preparation of PTh films is known as chronoamperometry to perform a film growth on top of the ITO covered substrate used as work electrode, based on the results of the CV on the polythiophene film was possible to determine that at a 1.9V potential, the film could be formed.

### 6.1.3. POLYTHIOPHENE/GRAPHENE OXIDE FILM SYNTHESIS

Chronoamperometry was used as the method to obtain GO/PTh thin films. Thin films were obtained applying a fixed potential of +1.9 V for 120 s. This potential corresponds to the oxidation of thiophene monomer determined by cyclic voltammetry. The increased current indicates the growth of the film over the ITO glass substrate.

### 6.1.4. POLYTHIOPHENE/GRAPHENE OXIDE FILM REDUCTION

A Cyclic Voltammetry is performed with the film to reduce the graphene oxide present in the film, the same arrangement of support electrolyte, work electrode, counter electrode, and reference electrode for the in-situ reduction. The difference was that when using aqueous electrolytes like sulfuric acid ($H_2SO_4$) or sodium sulfate ($Na_2SO_4$), the reduction of GO typically occurs in the range of approximately -0.2 V to -2.0 V vs. a reference electrode (e.g., Ag/AgCl).

The potential window you chosen should be optimized for specific experiments and considering the properties to achieve in the rGO. It's common to perform cyclic voltammetry (CV) or chronoamperometry experiments to determine the appropriate potential window and conditions for your electrochemical reduction process. Additionally, monitoring the current response during the reduction process can help you gauge the progress of the reaction.

## 6.2. CHARACTERIZATION

The crystalline structure of the samples was measured by X-ray diffraction (XRD) on a Bruker AXS diffractometer with a CuKα X-ray source (wavelength λ = 1.54184 Â) and a scan speed of 0.05º per minute. The range of the diffraction angle was 20º to 90º, this equipment is located in the Materials Laboratory III, F.C.Q., U.A.N.L.

The analysis by infrared spectroscopy (FTIR), on the graphene samples will allow to identify the functional groups present both in the GO and in the rGO, this equipment is located in the Materials Laboratory I, F.C.Q., U.A.N.L.

Field emission scanning electron microscopy (FESEM) was performed using a JEOL brand microscope with model number JSM6701F, with this technique the morphology and size of GO and rGO were determined.

Datos del TEM

Electrochemical measurements and synthesis were performed using a PGSTAT302N Metrohm Autolab. This device is in the Materials Laboratory I, F.C.Q., U.A.N.L.

# 7. RESULTS & DISCUSSION.

## 7.1. GRAPHENE SYNTHESIS

### 7.1.1. X-RAY DIFFRACTION (XRD)

X-ray diffraction measurements were carried out at room temperature using a Bruker AXS diffractometer equipped with a Cu Kα X-ray source (wavelength λ = 1.54184 Â) with a scanning interval of 2θ = ° 5 to 90 °. The data were acquired at a step size of 0.05 ° and a time of 4 s. The obtained diffraction patterns are presented in figures 3, 4, and 5 for G, GO, and rGO, respectively demonstrating different degrees of oxidation levels. As a starting point, an analysis of a graphite sample (see Figure 3) was performed to determine the changes with respect to the starting material.

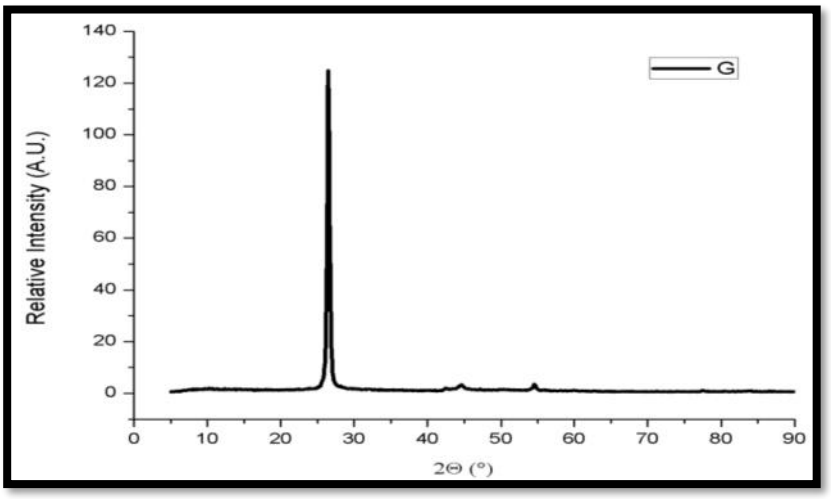


*Figure 3.- Graphite diffraction patterns.*

The graphite sample exhibits a strong and sharp peak at about 2θ = 26.5 °, corresponding to the (002) reflection plane, and two relatively weak intensity peaks at about 2θ = 44.5 ° and 54.5 º.

Compared to Figure 4 that presents the analysis performed for the GO sample, in which three characteristic signals are observed, and it is observed that after the oxidation process, the most intense peak is at an angle of 2θ = 10 °. Because the only procedures performed on this material were the oxidation reaction and the ultrasound treatment, the displacement of the signal with respect to the graphite signal (Figure 3) is attributed to the separation of the graphite layers, and these signals correspond to oxides of graphene, as reported in the work of Seehra et al.[58]. The presence of two very small peaks at approximately 2θ = 20 ° and 45 ° are both related to graphite and amorphous carbon species [58].

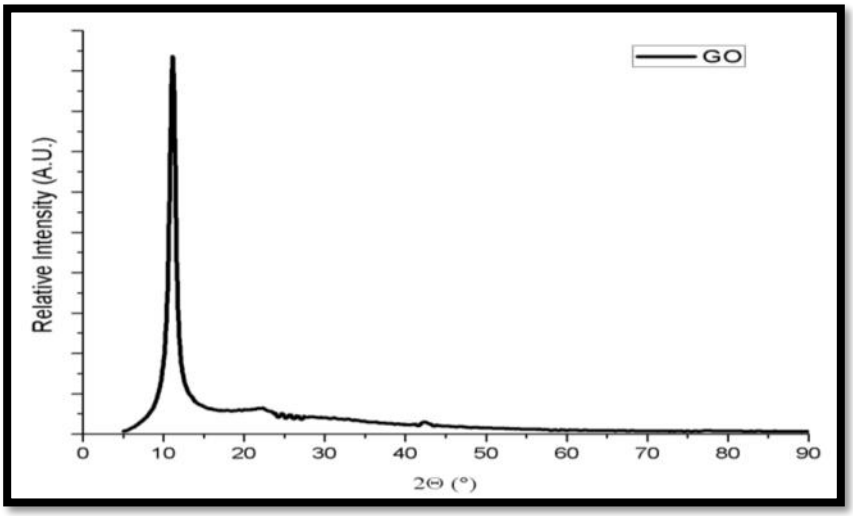


*Figure 4.- X-ray diffraction pattern of the GO sample.*

In the diffraction spectrum of rGO (Figure 5), three main signals were observed at 2θ = 10°, 24°, and 45 °. The signal of interest reported for the interpretation of this spectrum is that of the peak found in the range of angles 2θ = 45 ° to 47 °, since in literature it is mentioned that there are 4 reflections associated with conformations 2H (100), 3R ( 101), 2H (101) and 3R (012) for graphene[58]. The presence of a wide peak at angles close to 2θ = 24 ° is associated with signals from coke or activated carbon [58], and the peak observed in the spectrum at an angle 2θ = 10 ° is a characteristic peak for graphite [59].

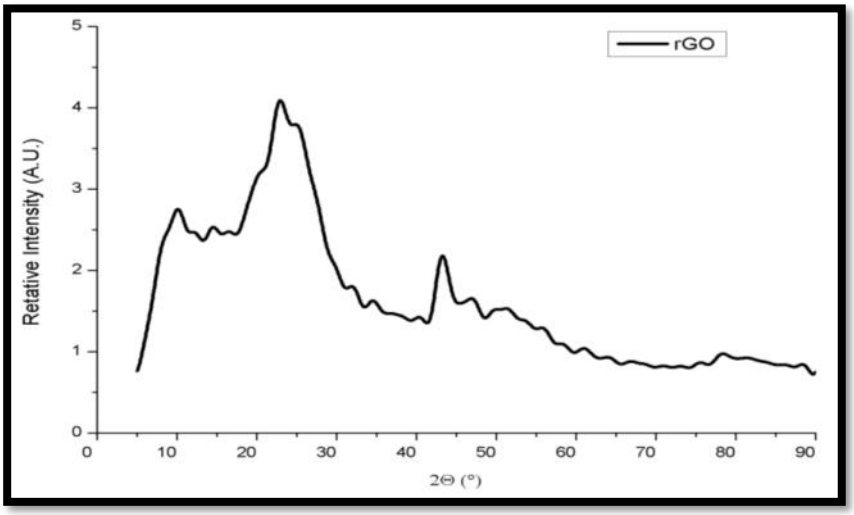


*Figure 5.- X-ray diffraction pattern of the rGO sample.*

### 7.1.2. INFRARED SPECTROSCOPY (FTIR)

In the FTIR spectrum shown in Figure 6, the results obtained for the samples of G, GO, and rGO are presented, in which a very clear difference can be observed between the GO line, Absorption peaks include a very intense band at 3425 $cm^{-1}$ which has the characteristic signal of the O-H stretching vibration of the COOH functional groups within the structure, and the line of the G, which does not present it, since it is the starting material.

While in the rGO this line is absent due to the reduction, which is done to eliminate said groups from the sample, while in the GO, some signals are also observed, weaker bands at 1720 $cm^{-1}$ and 1630 $cm^{-1}$ are attributed to the C=O stretching vibration of the carbonyl and the C=C stretching vibration, respectively, In addition, weak bands at 1400 $cm^{-1}$, 1228 $cm^{-1}$, and 1113 $cm^{-1}$ are responsible for O-H deformation, C-O stretching vibration of epoxy groups, and C-O stretching vibration of alkoxy groups, respectively[60].

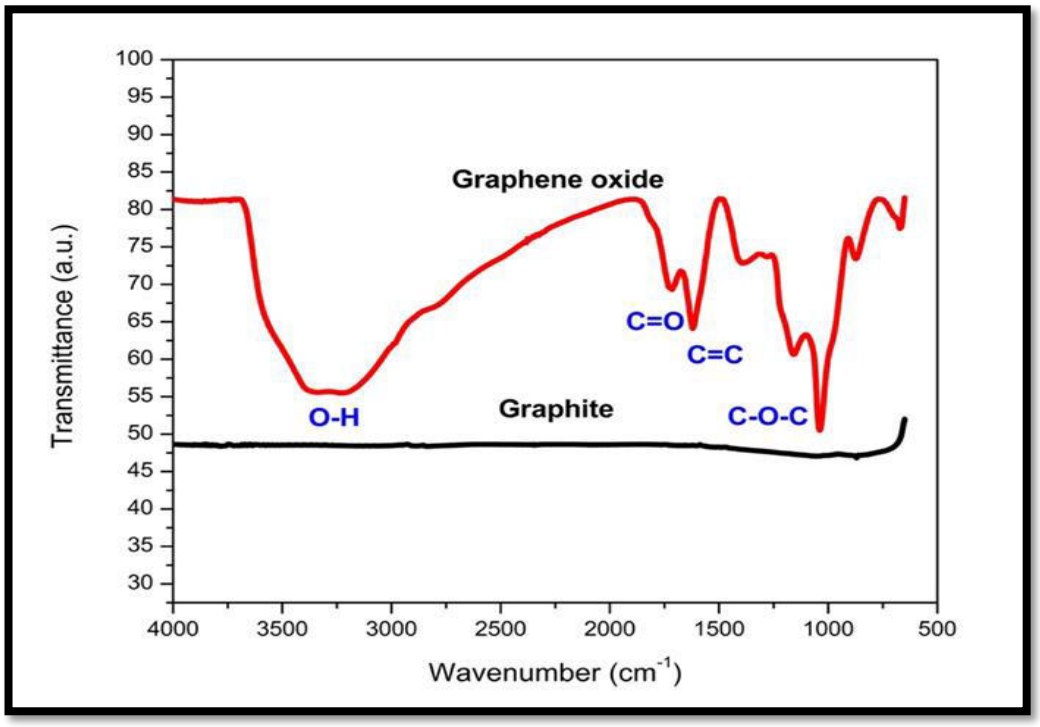


*Figure 6.- FTIR spectra of graphite (G), graphene oxide (GO) and reduced graphene oxide (rGO).*

Some of the signals present in GO appear to be present in the spectrum of rGO very weakly, which can be attributed to the fact that the reduction was not carried out completely and there may even be undesired functional groups present in the final product (Figure 7).

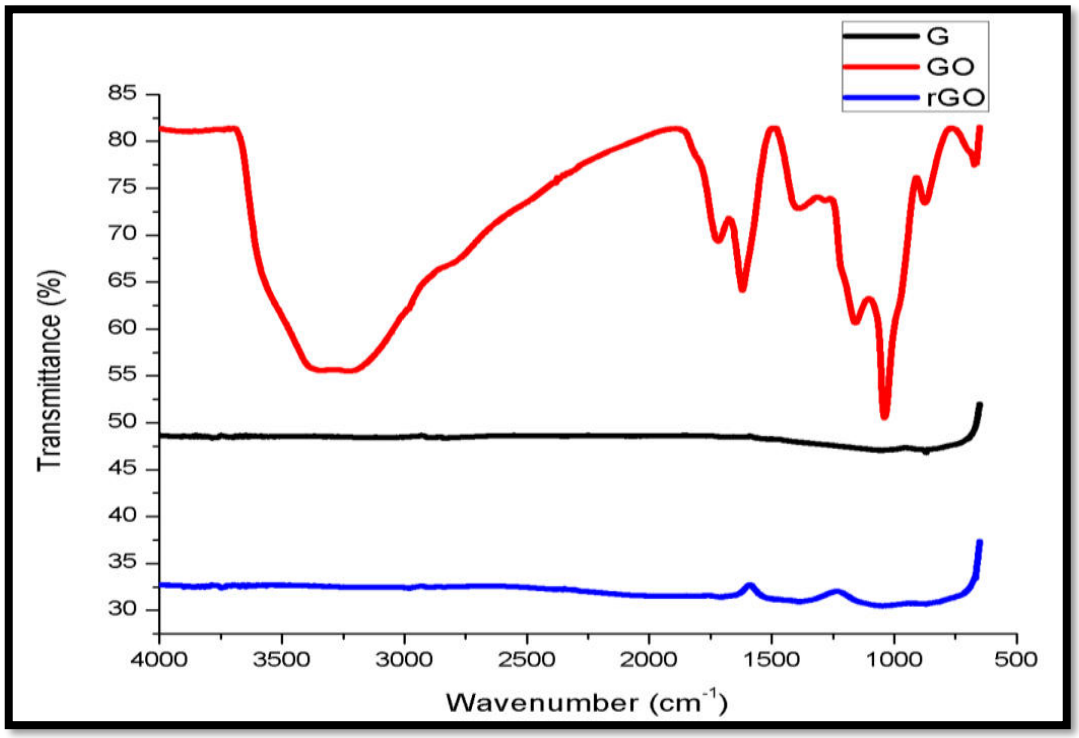


*Figure 7.- FTIR spectra of graphite (G), graphene oxide (GO) and reduced graphene oxide (rGO).*

### 7.1.3. FIELD EMISSION SCANNING ELECTRONIC MICROSCOPY (FESEM)

FESEM analyses were performed to analyze the morphology of the GO and rGO samples, as well as to observe the effect of reduction in the samples. The samples were deposited on aluminum-coated glass substrates and deposition was made by dripping and evaporating the sample on the surface with aluminum.

At first glance, in the micrographs presented in Figure 8, we can observe the layers of the GO with magnification x20,000 (A) and x27,000 (B), the separation of the layers can be seen in Figure 8 (B), whose separation is attributed to the oxidation of the graphite, which was then subjected to an ultrasonic bath to carry out the exfoliation.

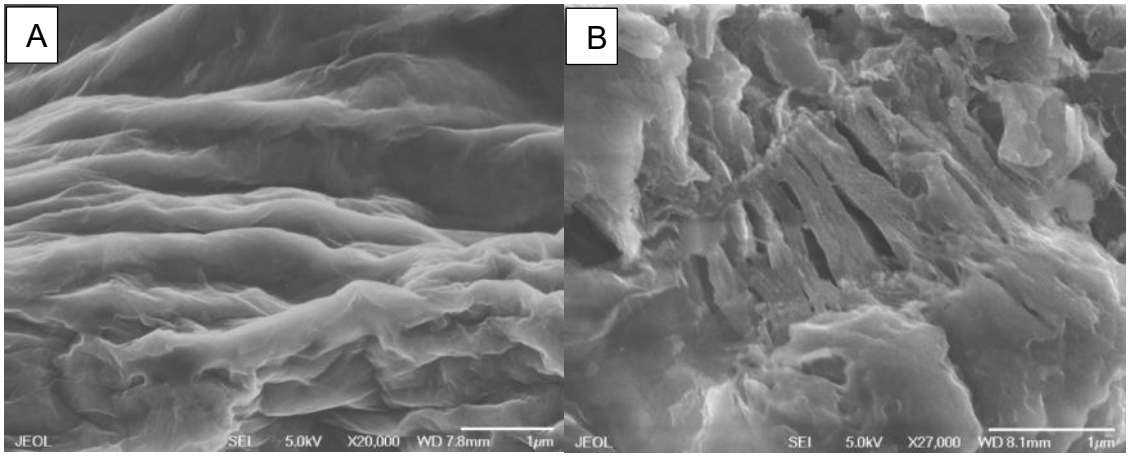


*Figure 8.- Micrographs of the GO sample.*

For the analysis of rGO samples, micrographs were obtained at x50,000 magnification, as shown in Figure 9, in which a separation in the layers of the rGO can be observed, which was expected from the synthesis process, although others are still required. analysis to determine the product quality and purity.

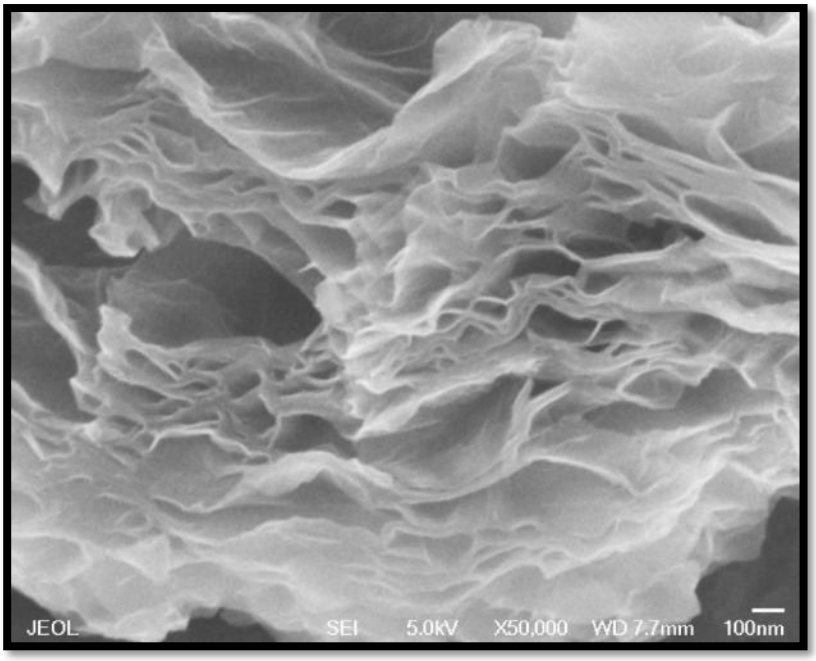


*Figure 9.- Micrograph of the rGO sample.*

### 7.1.4. X-RAY ENERGY DISPERSION SPECTROMETRY (EDS)

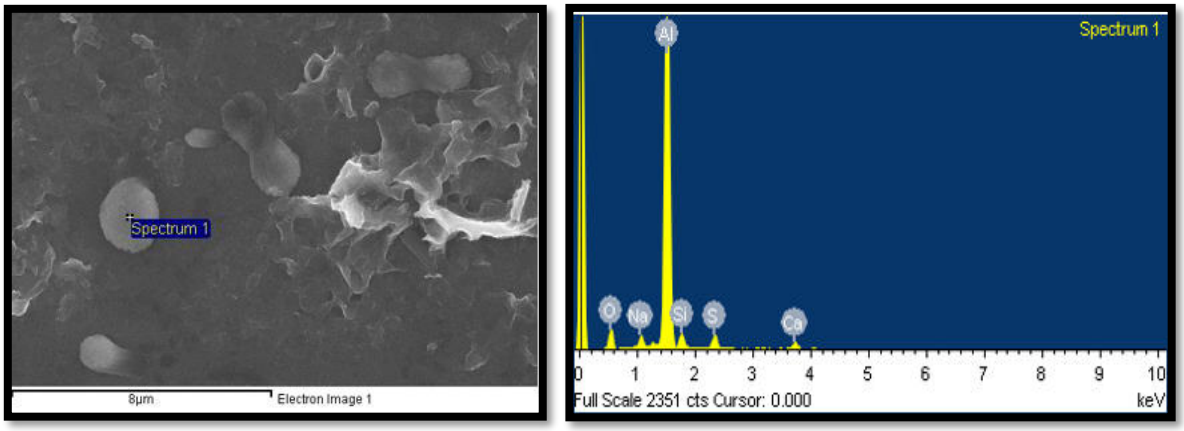


*Figure 10.- EDS analysis of the reduced graphene oxide sample.*

Elemental microanalyses were performed by EDS in graphene oxide samples, in Figure 10 the analyzed area is shown, as well as the result. This was done because of the presence of structures that could not be identified; however, using this technique, it was possible to identify sulfur crystals, which were possibly formed because they are residues of one of the acids used for the synthesis of graphene (sulfuric acid).

### 7.1.5. TRANSMISION ELECTRONIC MICROSCOPY

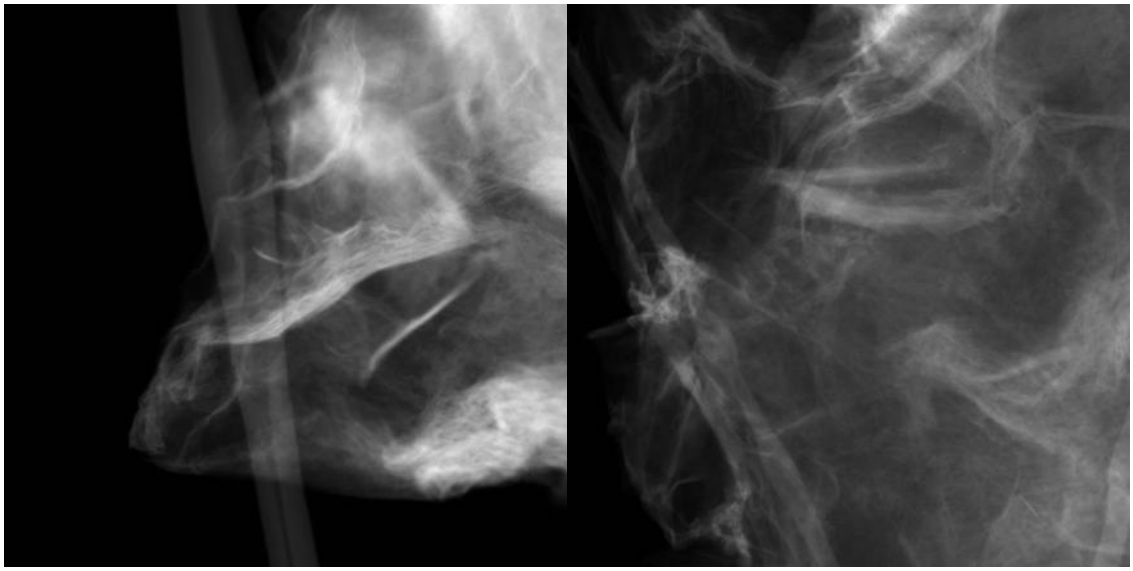

*Figure 11.- TEM analysis of graphene oxide (darkfield)*

As it was also seen in the SEM analysis the layers can be appreciated in this micrographs of GO which take us to the same conclusions on how the method can be improved to have a better layer separation maybe with the use of a probe ultrasound equipment along with improvement of the chemical oxidation, but there has to be a middle ground with both since that could also damage the lattices of carbon atoms to the point where sheet could be as small as necessary depending on the possible applications.

In Figure 11 we can observe the micrographs for the graphene oxide synthesized and a few of its morphologic characteristics. The sheets observed present a curly/wavy nature and some wrinkles can be observed in the surface of the graphene oxide sheets, this morphology could facilitate additional intercalation

cites for electrolyte ions or other types of particles, such as metallic nanoparticles, thus leading to a significant improvement in electrochemical performance. The higher the surface area the better since this could mean there's more accessible room for ion mobility.

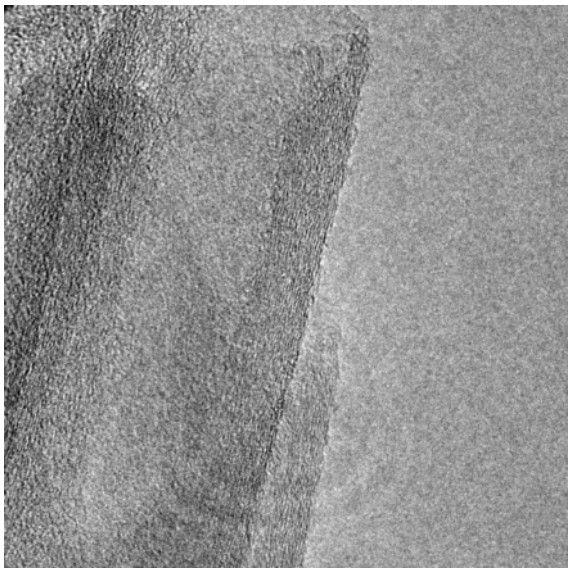

*Figure 12.- Graphene Oxide TEM (Brightfield)*

Heavier atoms scatter electrons more intensely than lighter atoms. In biological and polymeric samples with low atomic number, staining can help enhance the image contrast. Samples that are more crystalline are also more strongly diffracted and will appear darker in bright field mode, and brighter in dark field mode.

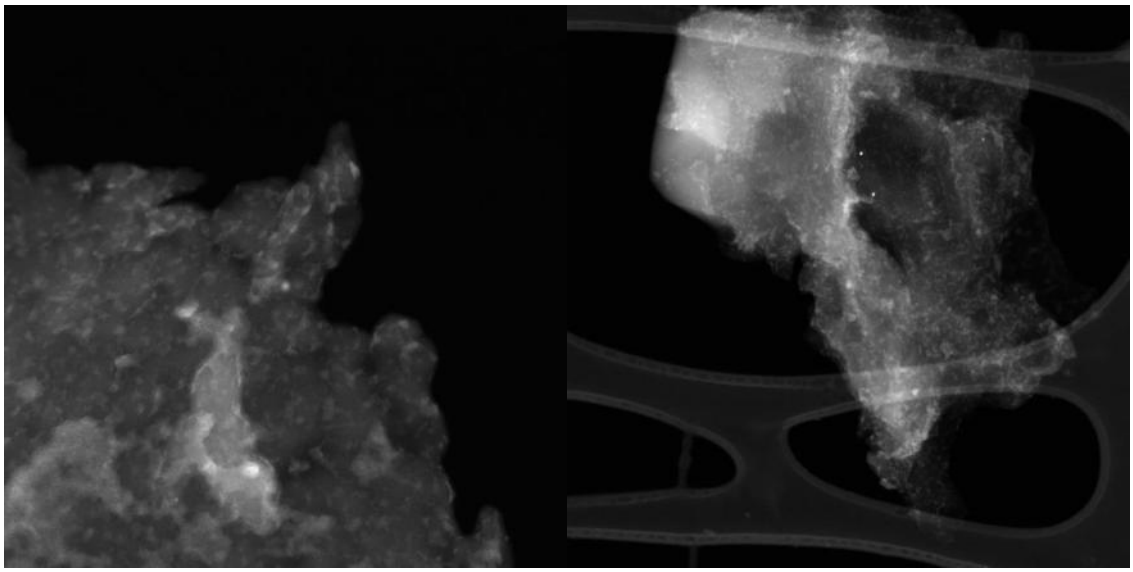

*Figure 13.- TEM analysis for graphene oxide/polythiophene film.*

The polythiophene/GO synthesized is in both images in Figure 13, where we can see a bit of the films amorphous surface and see some particles embedded in the film and they show a uniform distribution, there's also places where agglomeration is present, this behavior was also present in the films made only with polythiophene.

## 7.2. POLYTHIOPHENE FILM SYNTHESIS

Another proposed mechanism involves the electrophilic substitution of radical cations with neutral monomers to produce oligomers, which further oxidize and precipitate on the electrode surface[61].

The process of PTh film synthesis consists of first oxidizing the monomer by applying the appropriate oxidation potential, which favors the formation of monomer cations that concentrate on the surface of the working electrode and form a thin film. Doping and de-doping are reversible processes and do not degrade the polymer backbone. However, if a high potential is applied, conductive polymers undergo a not yet fully understood mechanism of over-oxidation, which is irreversible and causes rapid structural degradation and loss of electro-activity[62].

Furthermore, there's also a corresponding reduction peak corresponding to the reduction of the oxidized polymer into the neutral conjugated polymer that starts happening approximately at 1.4V where the polymer gains electrons, after this process is finished and potential reaches -0.6V another scan begins a new cycle to continue the polymer formation process and it can be performed in repetitions until the desired film thickness is reached or the polymer in the cell depletes, which in the voltammogram can be translated into a stalled current response to

the potential applied on the electrochemical cell and that's why the peak signals start to flatten as more cycles run for both oxidation and reduction peaks.

Another proposed mechanism involves the electrophilic substitution of radical cations with neutral monomers to produce oligomers, which further oxidize and precipitate on the electrode surface[61].

Furthermore, there's also a corresponding reduction peak corresponding to the reduction of the oxidized polymer into the neutral conjugated polymer that starts happening approximately at 1.4V where the polymer gains electrons, after this process is finished and potential reaches -0.6V another scan begins a new cycle to continue the polymer formation process and it can be performed in repetitions until the desired film thickness is reached or the polymer in the cell depletes, which in the voltammogram can be translated into a stalled current response to the potential applied on the electrochemical cell and that's why the peak signals start to flatten as more cycles run for both oxidation and reduction peaks.

The cyclic voltammogram for thiophene and $Bu_4NPF_6$ in acetonitrile solution obtained at 5 mV/s is shown in Figure 14. Voltammogram shows typical electrochemical behavior of PTh with an oxidation peak at +1.3 V associated with a p-doped state, functionalized polymers such as 3-bromo-4-dodecylthiphene has its oxidation peaks at +2.4V using the same support electrolyte showing that different reagents (halogenated thiophene monomer) could change the potential window for polymer formation[63]. The obtained thin films exhibit a thickness of 2.03 μm which can be controlled via reaction time and/or monomer concentration.

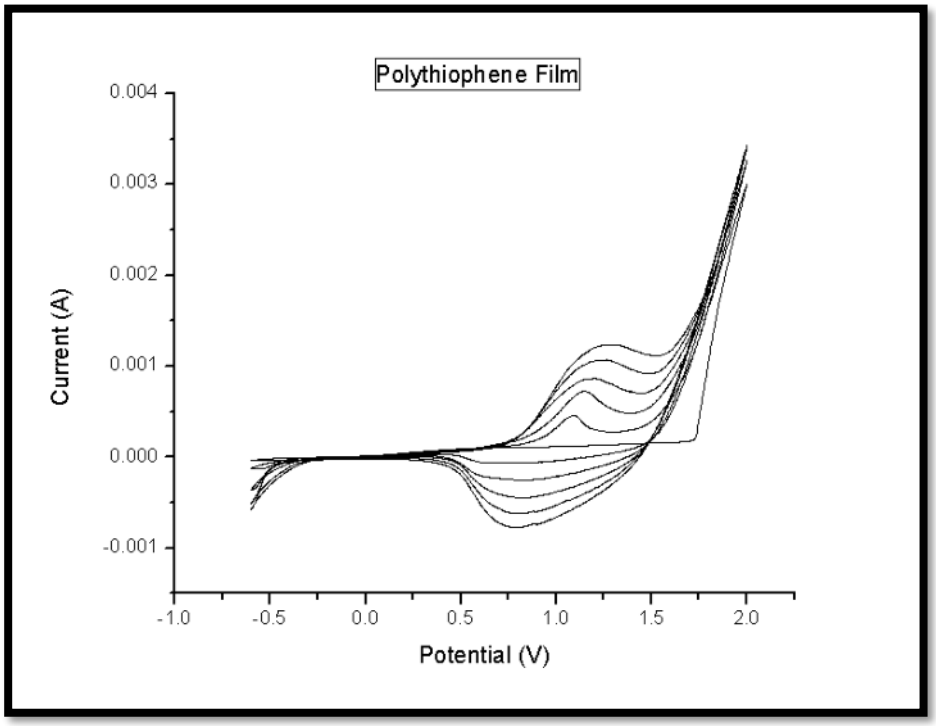


*Figure 14.- Cyclic voltammetry of polythiophene film*

## 7.3. POLYTHIOPHENE/GRAPHENE OXIDE FILM SYNTHESIS

PTh and PTh/GO thin films were obtained by chronoamperometry at a fixed anodic potential of +1.9 V, this increase in the potential needed to synthesize the film could be due to interference because of the presence of other substances (GO) in the electrochemical cell because with lower voltages the film wouldn't form on the substrate. Figure 15 shows the typical behavior for the electrodeposition of polythiophene, initial high current is associated with the oxidation and nucleation of the oligomer chains in the solution near the ITO surface. After nucleation, the current (2.7 mA) remained constant over time indicating the oligomer chains reached a molecular weight to precipitate on the electrode surface forming the PTh or PTh/GO thin films. The obtained thin films show a thickness of 2.42 µm. The thickness shows a time dependence, and with increasing time the film thickness also increases until reaching monomer depletion and oligomer precipitation.

Chronoamperometry was used as the method to obtain GO/PTh thin films. Thin films were obtained applying a fixed potential of +1.9 V for 120 s. This potential corresponds to the oxidation of thiophene monomer determined by cyclic voltammetry. The increased current indicates the growth of the film over the ITO glass substrate. The steep increase of current observed in Figure 15 at the beginning of the chronoamperometry run its attributed to the formation of the film

on the surface of the work electrode and the slow increase after is attributed to the growth of the film's thickness the longer the time runs on the experiment.

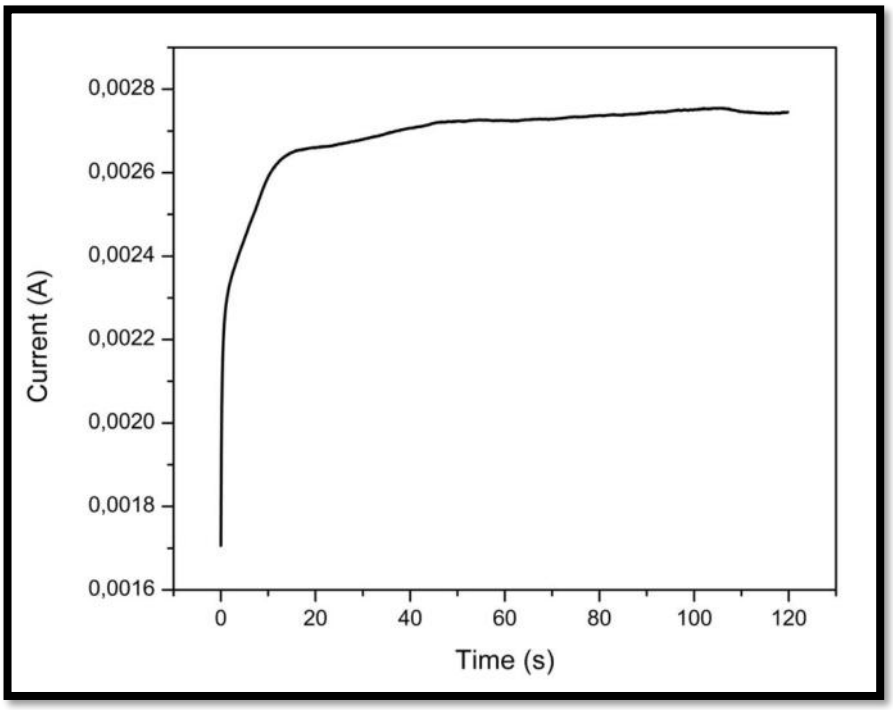


*Figure 15.- Polythiophene/Graphene Oxide Chronoamperometry Synthesis-*

As the film thickness have implications in different optoelectronic applications, it was determined using a profilometer. The thickness at different electrodeposition time is presented in Table 1. The thickness shows a time-dependence and as the time increases, film thickness increases as well reaching a maximum value of 2.84 $\mu m$.

*Table 1.- Thickness of PTh/GO films obtained by chronoamperometry.*

| Time(s) | Thickness (µm) |
|---|---|
| **200** | 2.42 |
| **400** | 2.67 |
| **600** | 2.84 |

Not only the thickness improves as times goes higher and higher, also the surface of the films has a more homogeneous distribution of polymer formed.

## 7.4. UV-VISIBLE ANALYSIS

UV-visible spectra of the samples are shown in Figure 16. The optical spectrum of PTh/GO shows a strong absorption at around 336 nm associated with $\pi$–$\pi$* transition while the strong absorption at around 485 nm is due to the bipolaron state of the polythiophene[64]. Bipolarons may result in the appearance of new absorption peaks in the UV-Vis spectrum that are not present in the spectrum of the neutral (undoped) polymer. The absorption bands of polarons are typically wider than those of neutral species and can offer insights into the charge carriers in the material[65].

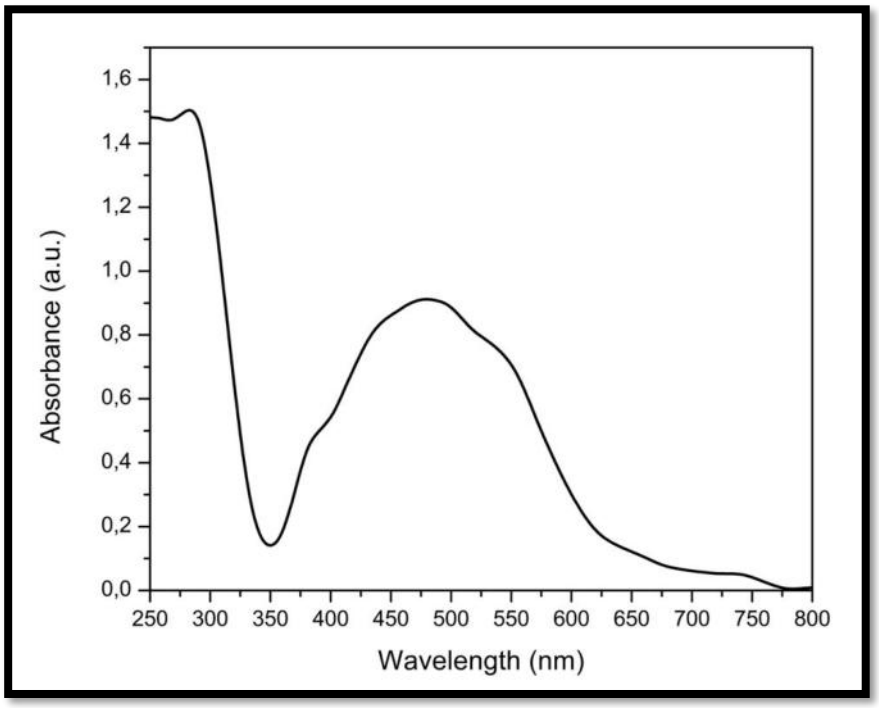


*Figure 16.- Absorption spectrum of PTh/GO on ITO substrate.*

## 7.5. PHOTOLUMINESCENCE ANALYSIS (PL)

The PL spectra of the PTh, GO, and PTh/GO thin films are shown in Figure 17. The composite film, upon excitation at 450 nm, showed three peaks at 496 nm, 536 nm, and 612 nm. The three peaks are associated with σ*-n, $\pi$–$\pi$* and $\pi$*-n electronic transitions, respectively. A broader peak due to $\pi$–$\pi$* emission was observed for the composite films associated with the $sp^2$ carbon atoms from both graphene oxide and polythiophene. A conjugated polymer, such as polythiophene, can display redshifts in its absorption peaks, which are influenced by factors such as molecular structure, conjugation length, excitation energy and interactions with other materials. This phenomenon has significant implications for their application in organic electronics and optoelectronic devices[66].

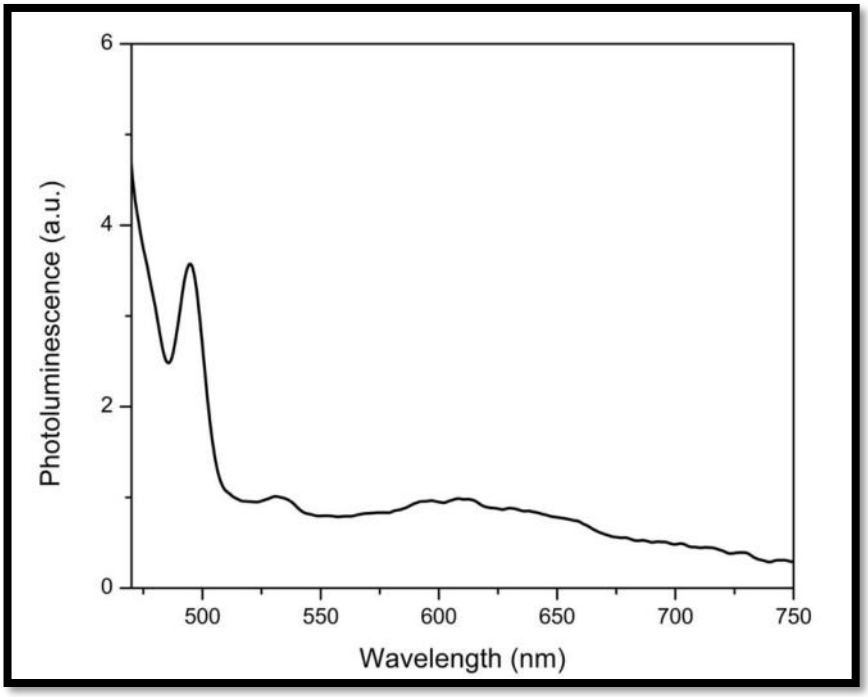


*Figure 17.- Emission spectrum of PTh/GO on ITO substrate.*

# 8. CONCLUSIONS

- The FESEM analysis of the graphene allowed the identification of the morphology of agglomerated layers, and in recent experiments, it was observed that the method for recovery of the product improved by not filtering it but using a centrifuge, this allowed better observation of the rGO (chemically reduced).

- By means of the structural analysis of graphene, impurities related to the presence of oxidized graphene species as well as rGO are presented, which is why it is necessary to study the parameters that influence the formation of pure graphene in the chemically reduced samples for this reason this method wasn't explored any further.

- The tests for the synthesis of polythiophene were carried out as reported, but because the results were not similar to those reported, it is concluded that there may be an intermediate step that were not reported for obtaining the films, and an analysis should be carried out in depth of the method used to obtain polythiophene films.

- XRD analysis of the synthesized reduced graphene oxide allowed us to identify the presence of the oxidized species of graphene as well as rGO.

- Ultrasonic bath could be replaced with an ultrasonic probe to improve the separation of layers of the GO.

- The FESEM analysis of the synthesized graphene allowed us to identify it in the form of agglomerated layers.
- The handling of the graphene oxide after being synthesized affects drastically it's capabilities to form homogenic layers of PTh/GO films if particle size remains too big it may act as place for PTh to grow before becoming part of the film itself.
- Tinkering with the conditions in the electrochemical reduction for graphene oxide could maybe improve on its morphology and could also improve the layers separation, which could at the same time improve the electric properties of the films.
- The thin films showed optical absorption at 366 nm and 485 nm due to the $\pi$–$\pi^*$ transition and the bipolaron state of the polythiophene. While the emission properties indicate a strong $\pi$–$\pi^*$ emission due to $sp^2$ carbon atoms present in graphene oxide and polythiophene.
- The effect of the thickness over the electrodeposition time was also investigated and showed that it will continue to grow until monomer/oligomer depletion.
-

# 9. SCHEDULE

*Table 2.- Proposed Schedule*

| *Activities* | *1st Semester* | *2nd Semester* | *3rd Semester* | *4th Semester* | *5th Semester* | *6th Semester* |
|---|---|---|---|---|---|---|
| Literature Research | | | | | | |
| Research Protocol | | | | | | |
| Gold Nanoparticles Synthesis | | | | | | |
| Graphene Synthesis | | | | | | |
| Film Synthesis and Deposition | | | | | | |
| Characterization | | | | | | |
| Conductivity Evaluation | | | | | | |
| Results Evaluation | | | | | | |
| Research Paper Sent | | | | | | |

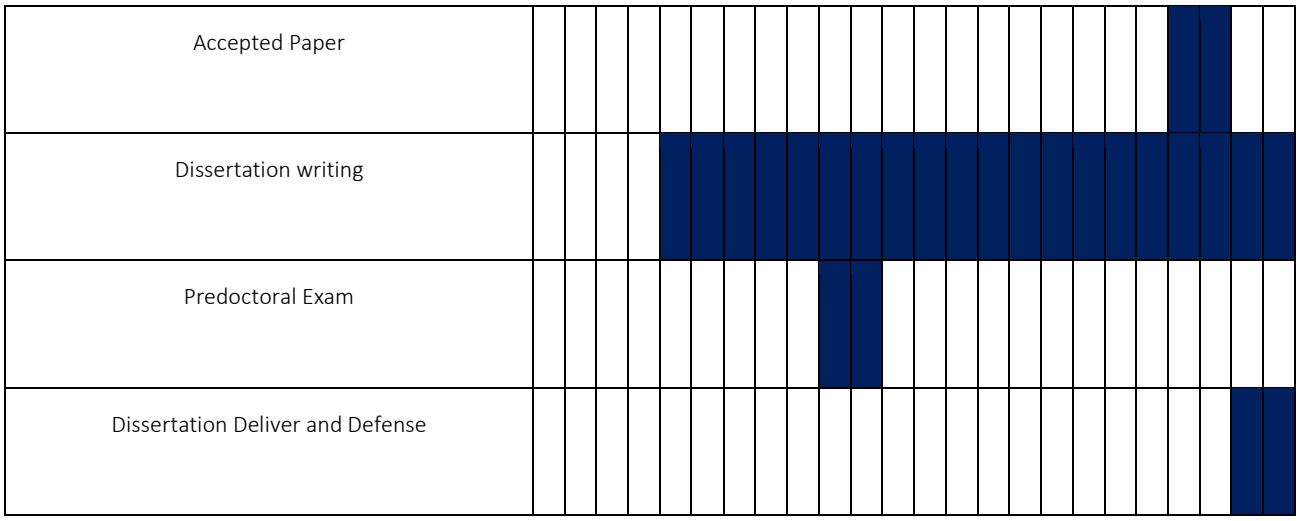


## 10. RESIDUE DISPOSAL

The elimination of waste will be carried out in accordance with the regulations of the Faculty of Chemical Sciences of the Autonomous University of Nuevo León.

The gold experiments were deposited in container F, corresponding to the recycling of the precious metals. The waste generated from the halogenated solvent waste will be deposited in container D.

## 11. ACKNOWLEDGEMENTS

Special thanks to CONACYT for the scholarship and support registered with project number PN150.

# 12. FIGURES AND TABLES

## 12.1. TABLES



## 12.2. FIGURES

# 13. ANNEXES

## 13.1. METALLIC NANOPARTICLES BACKGROUND

Many synthesis methods have been reported for the preparation of metallic nanoparticles, and Fanta et al.[57] synthesized AgNPs that were stabilized using starch.[67] Their results show that multiple techniques have been characterized, including atomic emission spectroscopy of inductively coupled plasma (ICP-AES), UV-VIS spectroscopy, X-ray diffraction (XRD), transmission electron microscopy (TEM), scanning electron microscopy (SEM), and optical microscopy [67].

A study by Chandra et al. The synthesis of copper nanoparticles was achieved by reducing the solution. The influence of the parameters on the size of the copper nanoparticles was studied, and process referential parameters were obtained. The morphology and structure of the synthesized copper nanoparticles were characterized using transmission electron microscopy (TEM), X-ray diffraction (XRD), quasi-elastic light scattering (QELS), infrared spectroscopy (FTIR), and solid-state UV spectroscopy. It was found that the average size of nanoparticles was 15 ± 2 nm.[68].

Based on the aforementioned research reports, the methods for the preparation of the samples for the characterization techniques, as well as some of the key

points for the interpretation of results, will serve as a guide for the analysis of the results obtained from the research process.

In relation to the obtaining of metallic nanoparticles, the working group of Zhao et al. reports a simple method of synthesis of silver nanoparticles. Sodium alginate was used as the stabilizer and reducer. In the same study, a possible mechanism for the reduction and stabilization of nanoparticles was investigated. The solution was sodium alginate, which was dissolved in distilled water in a 100 ml beaker using a magnetic stirrer on a heating plate. After complete dissolution, the pH of the solution was adjusted to within the range of 5-11. After adding a certain amount of precursor dropwise, $AgNO_3$ was added (considering that the total volume of the reaction medium was 25 ml). As a result, they report that they obtained nanoparticles with a size in the range of 10 to 20 nm, varying the conditions such as pH, the concentration of sodium alginate and the concentration of $AgNO_3$ [46].

Similarly, Valdez et al. reported the microwave-assisted synthesis of metallic nanoparticles using L-cysteine and sodium alginate as reducing and stabilizing agents, respectively, as a solvent medium using ethylene glycol. They observed by means of a statistical analysis the interactions that the established variables had with respect to the obtaining of the characteristic plasmon for the metallic nanoparticles of Au, Ag and Cu analyzed by means of the technique of UV-Vis spectroscopy. The variables considered for this experiment were the concentration of cysteine, the time that the sample would pass the microwave treatment, and the pH. The synthesis of nanoparticles was carried out after a

design of experiments to acquire different metal nanoparticles using two parameters: the reaction time in the microwave and the concentration of metal [69].

Tanabe et al., Conducted research on the effects of the morphology and size of gold nanoparticles on the photocatalytic properties of TiO2. In this study, we report the absorption spectra of anatase and rutile TiO2 modified with Au nanospheres of (5-60 nm) in the wavelength region from 150 to 300 nm using attenuated total reflection spectroscopy. They also reported that smaller Au nanospheres induced a greater spectral change, which means large changes in the electronic state and improved the efficiency of load separations. The photocatalytic activity in their experiments showed their dependence on the size of the Au nanospheres; thus, it was determined that the nanoparticles of TiO2 of smaller size showed the highest photocatalytic activity. The photocatalytic activity was calculated from the degradation of methylene blue solutions [5].

Subrahmanyam et al. demonstrated the experimental procedure of synthesis and characterization to produce a uniform coating of spherical gold nanoparticles on a sheet of graphene. The UV-Vis spectrum of the nanocomposite obtained shows the characteristic surface plasmon resonance band due to the Au nanoparticles at approximately 530 nm [31].

## 13.1. GOLD NANOPARTICLES (AUNPS)

Noble metal nanoparticles and their bright colors owing to the absorption of surface plasmon resonance ("SPR") constitute a large field of research [70]. The color of nanoparticles depends on the shape and size of the nanoparticles and the dielectric constant of the surrounding medium, which has led to many studies on their synthesis and applications[7,8,10,33,39,40,71–85].

The difficulty in generating the desired size, shape, and monodispersity of nanoparticles continues to pressure the need to develop new and refined synthesis methodologies with respect to the quality and desired characteristics of the material. The formation of chemical and physical interfaces that allow interaction with target molecules also drives the need to develop various synthesis techniques for the generation of metallic nanoparticles [80].

In the literature we report, in a historical way, methods to generate wonderfully colored glass by adding gold to generate burgundy, reds, or purples. Faraday attributed this color to very finely divided colloidal gold, or gold nanoparticles as it is known today [78,86,87]. As the size or shape of the nanoparticle changes, the observed color also changes as well as the characteristic signal in UV-Vis spectrometry [72,88]. The gold spheres have a characteristic red color, while the silver spheres are yellow. Latest studies [40,69,71,79,80,85,88] have shown that the color is due to the collective oscillation of the electrons in the conduction band, known as SPR [71]. The oscillation frequency is generally in the visible region for

gold and silver resulting in a strong absorption of surface plasmon resonance. Therefore, the origin of the optical and conductive properties that they present at the nanoscale are different for metal nanoparticles compared to semiconductor nanoparticles.

The metal nanoparticles of Au have been recently studied with the purpose of improving the electronic interaction between different materials, also studying the effects of morphology and particle sizes. For example, in the literature it is reported that the absorption spectra of anatase and rutile films $TiO_2$ modified with several sizes of nanobeads of Au 5 - 60 nm, were analyzed in the wavelength spectrum region of 150 to 300 nm, measuring them by means of attenuated total reflection spectroscopy, indicating that the smaller Au nanospheres induced greater spectral changes, which meant greater changes in the electronic state and greater effects in the load separation efficiency [5].

## 13.2. CRITICAL ANALYSIS

In previous research, both graphene and Au nanoparticles, they have been given many and different applications, for the gold nanoparticles research has been done in which its purpose is to use it as: repellent / pesticide [84], medicine (cancer therapies)[89], chemical/biologic sensor [74], etc. For its part, graphene is being used as: biosensor [9], 3D printed circuitry [53], flexible electronics like transistors, in fuel cells, energy storage [7], drug delivery [8], etc. In addition, to graphene particles either in combination with other substances such as metals or other compounds, some of the uses reported are detector (G-Au)[33], flexible electronics (G-Polymer)[7,12] , adsorbent (G-polyamide)[29], etc. Alginate-based biocomposites are used in food packaging, tissue engineering, biomedicine, pharmaceutical fields due to their non-toxicity, biodegradability, and biocompatibility [69,90,91].

## 13.1. GOLD NANOPARTICLES SYNTHESIS (AUNPS)

### 13.1.1. CONVENTIONAL HEATING METHOD

For the synthesis of Au nanoparticles, the Turkevich methodology was used [71]; 1 ml of a 25 mM $HAuCl_4$ solution was taken, and 100 ml will be added. This solution was left under stirring and heating until it boils. Then, 5 ml of 1% by weight of sodium citrate was added; the solution, originally yellow, becomes colorless and finally vinaceous red[73]. The solution is left to boil for 30 minutes and finally was gauged to 100 ml to compensate for evaporation losses. All this process can be seen in the representation shown in Figure 18.

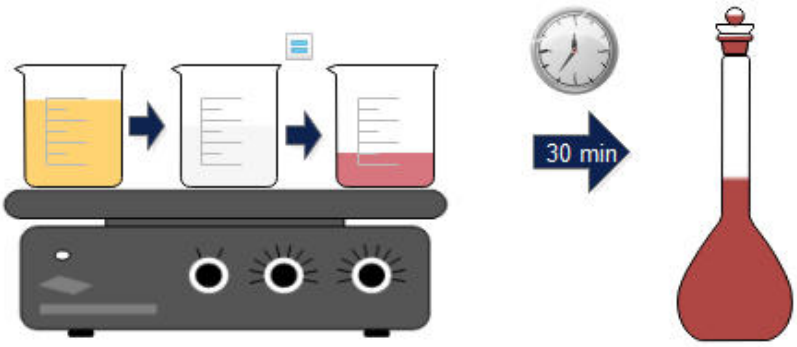


*Figure 18.- Conventional Heating Gold Nanoparticles Synthesis Scheme*

### 13.1.2. MICROWAVE ASSISTED

For the microwaves assisted synthesis method, 1ml of a solution of $HAuCl_4$ with a concentration of 5mM was taken, to observe the effect of the citrate concentration this was varied to 10, 20 and 30 mM adding 1ml in the experiments, these are dissolved with 18 ml of water and the solution inside a beaker is placed inside a conventional microwave oven which operates at 20% of its maximum power (1275W), was carried out by cycles of heating of 2, 5 and 10 cycles that in total they took a time of 10 minutes. The outline of the experimental procedure to be followed is shown in Figure 19.


*Figure 19.- Microwave Assisted Gold Nanoparticles Synthesis Scheme*

## 13.1. GOLD NANOPARTICLES SYNTHESIS (AUNPS)

The synthesis of the gold nanoparticles was carried out with the procedure established in the conventional heating methodology and also by the microwave assisted synthesis method with which different distributions of particle sizes were obtained which were analyzed using the DLS equipment and also by UV-vis spectroscopy. Figure 20 shows the photographs of the samples obtained (B and C) in comparison with reported ones (A), which as reported have different colorations which are related to the size of particles obtained, this change in color is due to the SPR of the particles interacting with the light absorbing different Wavelengths according to their size and thanks to this, their size can be estimated using the UV-Vis spectroscopy technique, comparing with previously reported results in the literature.

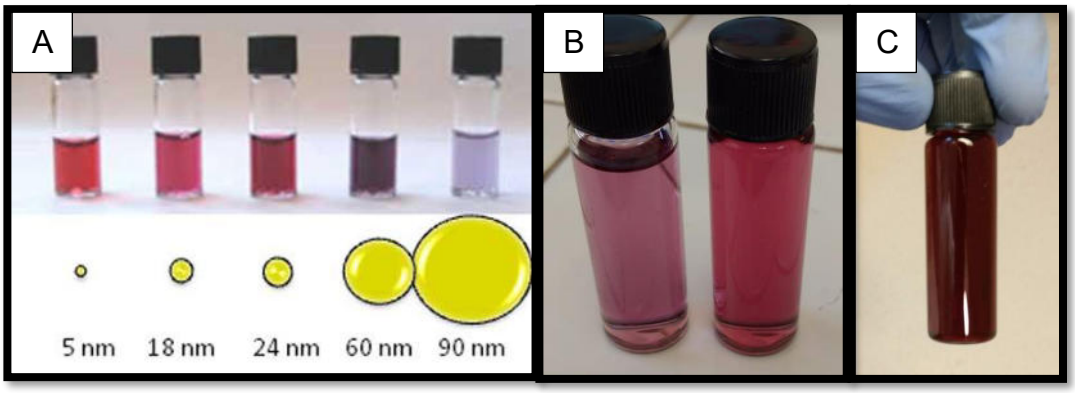


*Figure 20.- Synthesized Gold Nanoparticles*

## 13.1. CHARACTERIZATION OF GOLD NANOPARTICLES

The characterization of Au nanoparticles, graphene, as well as the films obtained were be made by using the following analysis techniques:

Dynamic Dispersion of Light (DLS), will be used to observe the distribution and size of Au nanoparticles, this equipment is available in Materials Laboratory I, F.C.Q., U.A.N.L.

For morphology examination of the Au nanoparticles, the techniques of scanning electron microscopy by field emission (FESEM) and transmission electron microscopy (TEM) were be used. The first one is in the Advanced Microscopy Laboratory of the FCQ, UANL., And in the case of TEM, this team is in the Center for Innovation, Research and Development in Engineering and Technology (C.I.I.D.I.T.) of the F.I.M.E., U.A.N.L.

To characterize the Au nanoparticles, the localized surface plasmon resonance (LSPR) of the synthesized nanoparticles was analyzed using a UV-Vis spectrophotometer. This device is in the Materials Laboratory I, F.C.Q., U.A.N.L.

## 13.2. CHARACTERIZATION RESULTS

### 13.2.1. DYNAMIC LIGHT SCATTERING ANALYSIS (DLS)

According to the results obtained by the DLS analysis, it was determined that the particle sizes obtained in both syntheses varied according to the heating method used to produce them, in the case of the gold nanoparticles they had a size distribution of 20 ~ 60 nm (as shown in Figure 21) in the case of those synthesized via conventional heating.

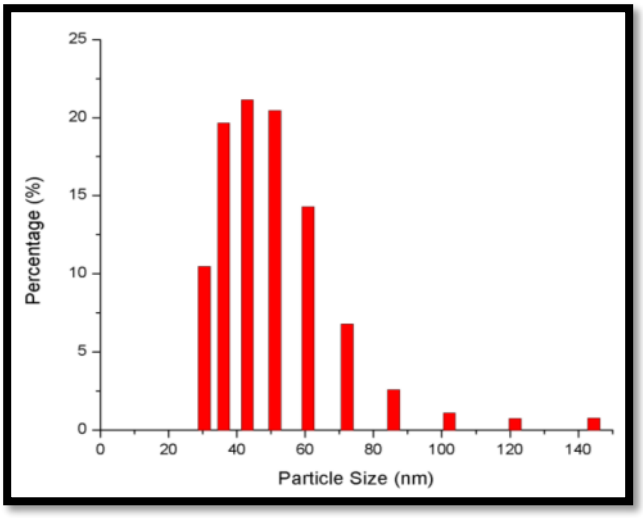


*Figure 21.- Particle size distribution, Sample of gold nanoparticles synthesized by conventional heating*

The difference in size is attributed to the way in which energy is supplied to the system, since by conventional heating a temperature gradient is created from the bottom of the vessel to the liquid surface, while in microwave synthesis the liquid

it is irradiated and the energy necessary to carry out the synthesis reaction is supplied in a more uniform way. The supply of energy to the system directly affects the range of sizes obtained for the samples, this also directly affects the stability of the nanoparticles since the AuNPs synthesized by the microwave method tend to have a lower stability and end up precipitating before the synthesized by the conventional heating method.

### 13.2.2. UV-VIS SPECTROSCOPY

Figures 22, 23 and 24 show the UV-Vis spectra obtained for the different experimental configurations carried out for the purpose of synthesizing Au nanoparticles by means of microwave-assisted heating.

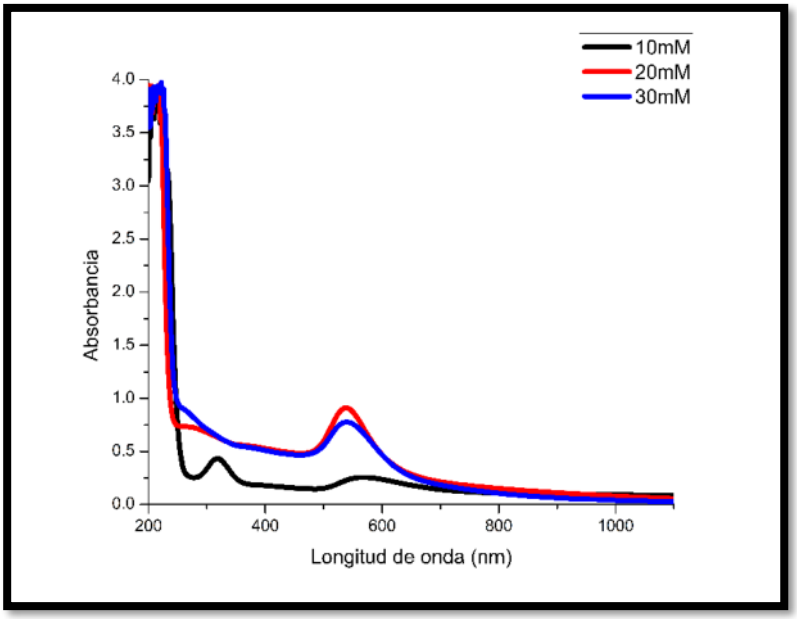


*Figure 22.- Microwave synthesis with 2 heating cycles, different concentrations of sodium citrate.*

In the investigation of Thanh et. to the. in which they use a microwave synthesis method of AuNPs it is reported that the wavelengths of maximum absorbance (λmax) for the AuNPs are between 518 ~ 524 nm with a size of 12-25 nm. The size of the AuNPs decreases with the increase in the concentration of sodium citrate, in addition, the conditions for carrying out the synthesis were based on

this document [79]. While in the case of the experiments carried out, increasing the sodium citrate concentration defined the plasmon characteristic signal a little more, while decreasing it to 10 mM, it was affected in a negative way, lowering the absorbance significantly with respect to the concentrations of 20mM and 30mM as presented in Figures 22, 23 and 24.

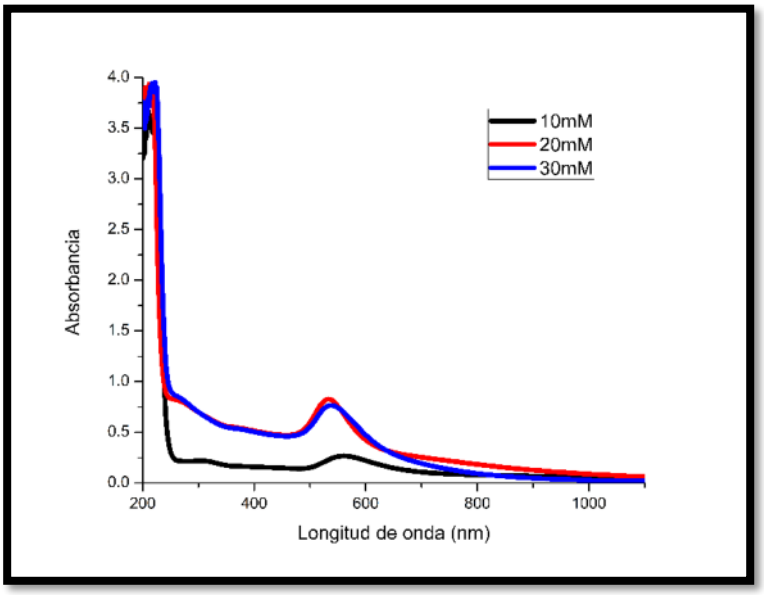


*Figure 23.- Microwave synthesis with 5 heating cycles, different concentrations of sodium citrate.*

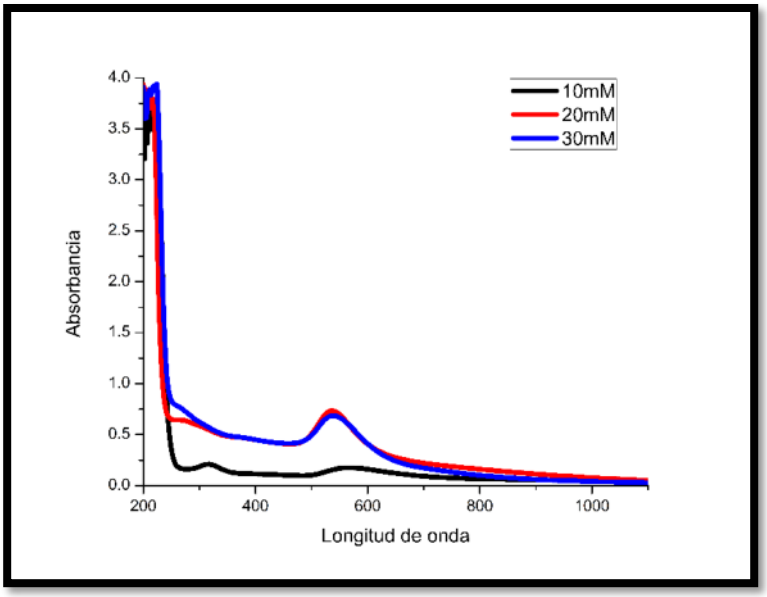


*Figure 24.- Microwave synthesis with 10 heating cycles, different concentrations of sodium citrate.*

The obtained results of UV-Vis absorbance allow us to infer that Au nanoparticles were obtained, as reported in the work of Valdez et. al., who identified at a wavelength of 524 nm the presence of gold nanoparticles, in that work they used L-cysteine as a reducing and stabilizing agent [69].

Based on the best results presented for both synthesis of gold nanoparticles (conventional heating and microwave assisted Figures 25 and 26 respectively), the choice of samples for future analysis was made.

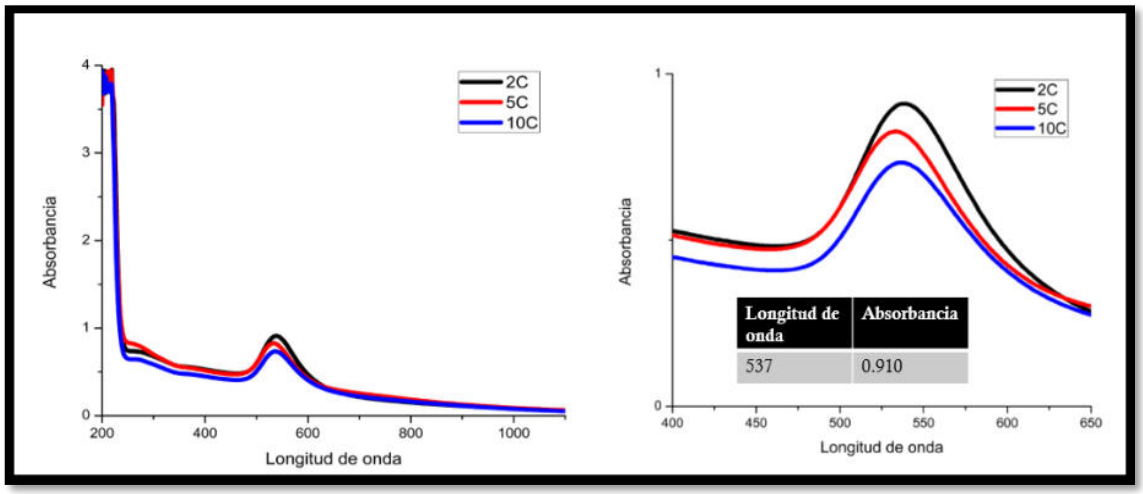


*Figure 25.- Comparison according to microwave heating cycles, using the same concentration of sodium citrate (20mM) (A) and an approach to observe the band of higher absorbance obtained in tests (B).*

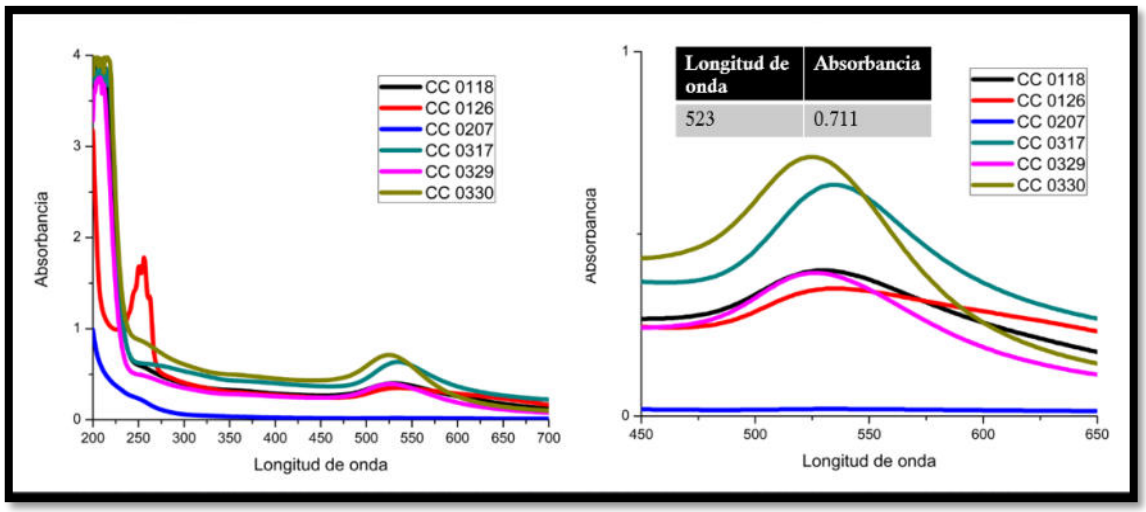


*Figure 26.- Comparison of absorbances in experiments using the conventional heating method (A) and an approach to observe the band of higher absorbance obtained in tests (B).*

Another method explored in the synthesis of AuNPs involved modifications wherein tannic acid was employed to regulate the growth of AuNPs, resulting in the most favorable outcomes with minimized dispersion and overall smaller sizes. This observation correlates with the observed maximum absorbance peak depicted in Figure 27, wherein, compared to other methods, there is a shift towards shorter wavelengths, indicating enhanced efficiency.

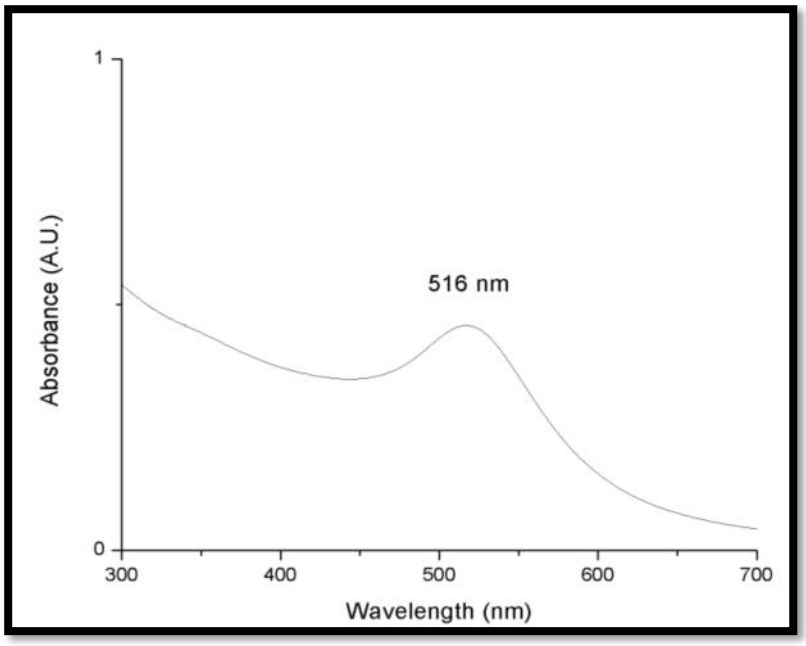


*Figure 27.- Au nanoparticles synthesis using the upgraded method with tannic acid.*

### 13.2.3. FIELD EMISSION SCANNING ELECTRONIC MICROSCOPY (FESEM)

In Figure 28, a micrograph of FESEM obtained at 100000X in secondary electron mode is shown, for a sample of AuNPs synthesized by the microwave-assisted Turkevich method, in which individual nanoparticles are observed from 14nm to 36nm, as well as multiple particles that appear to be formed by agglomeration.

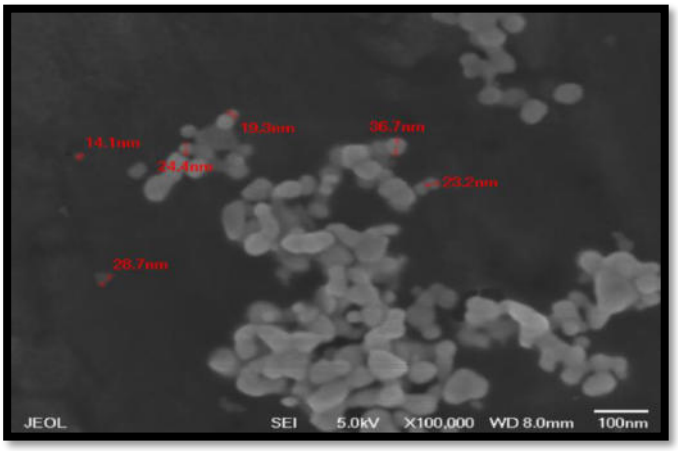


*Figure 28.- FESEM AuNPs 2C MW*

On the other hand, in Figure 28 a micrograph of FESEM in the secondary electron mode of a sample of synthesis of AuNPs performed by conventional heating method is presented, in this image very small particles are seen along with agglomerations of sizes up to 100 nm. In these, sizes obtained between 5 to 20 nm are estimated.

According to these results, as well as that observed by UV-Vis spectroscopy, it can be inferred that the AuNPs synthesized by microwaves, which showed a higher absorbance (observed in the UV-Vis spectroscopy analysis), which is directly related to their size, could lead to an improvement of the exciton-plasmon interactions for the conformation of a conductive film.

In Figure 29 another synthesis method was executed in order to optimize the size distribution and the effects of tannic acid are easily observed due to the narrowing of particle size distribution (10~25 nm).

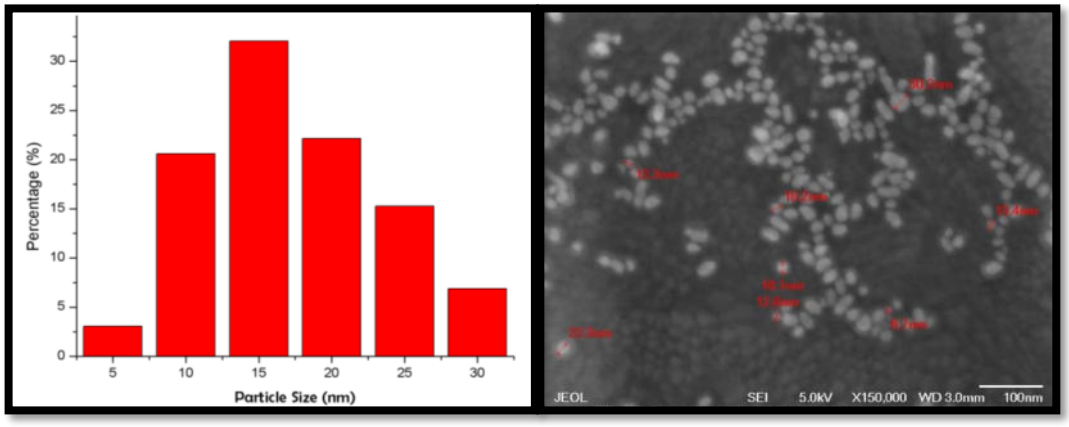


*Figure 29.- Particle Size Analysis In FESEM micrography.*

### 13.2.4. X-RAY ENERGY DISPERSION SPECTROMETRY

To verify that the nanoparticles identified by FESEM were Au nanoparticles, an elementary microanalysis by EDS was performed on these samples. **¡Error! No se encuentra el origen de la referencia.** shows a micrograph of one of the analyzed areas as well as the spectrum of EDS obtained, where it is identified as Au; It should be mentioned that the detected Al belongs to the support on which Au nanoparticles were deposited for analysis by FESEM.

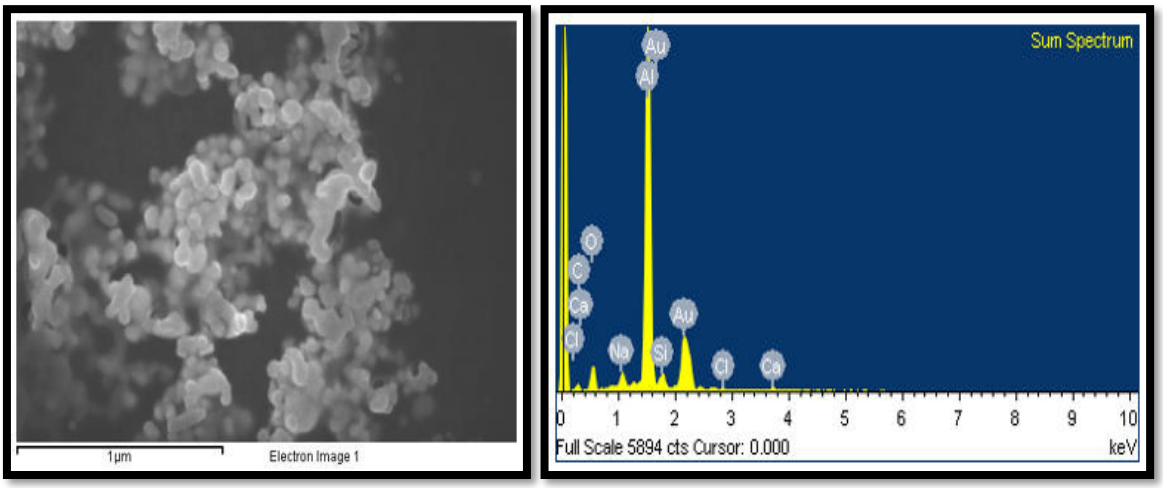


*Figure 30.- EDS Analysis of Gold Nanoparticles.*

### 13.2.5. TRANSMISION ELECTRONIC MICROSCOPY

Since heavier atoms scatter electrons more intensely than lighter atoms, an increased presence of crystalline spots is discernible on the film surface in this sample. These spots exhibit stronger diffraction and thus appear darker or brighter in dark field mode.

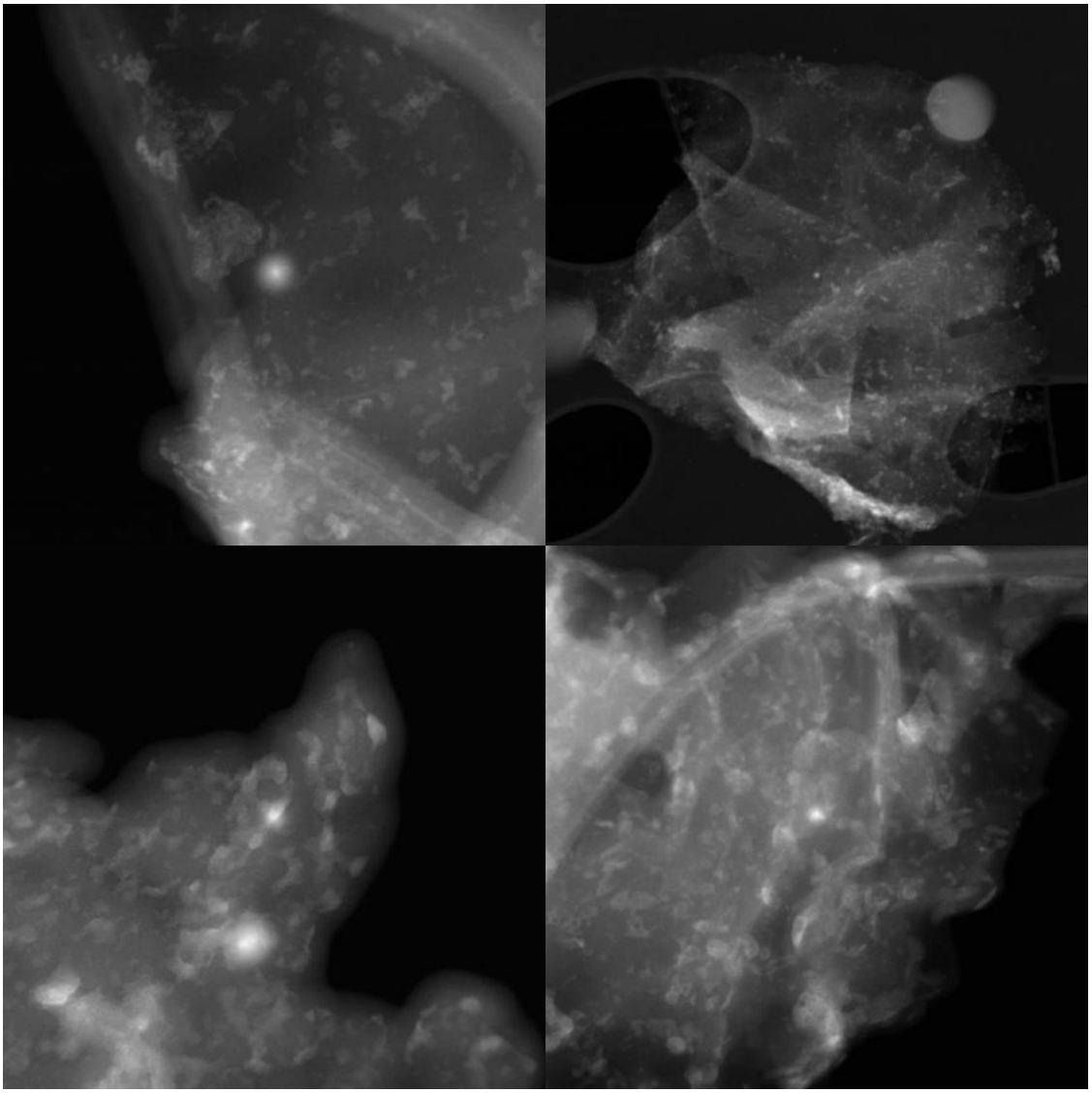

*Figure 31.-TEM images for the rGO/PTh/AuNPs films.*

Following this reasoning, the presence of gold nanoparticles on the surface, along with the behavior previously observed with the polythiophene film and graphene oxide, provides the sole plausible explanation for these spots. The gold nanoparticles were intentionally deposited to decorate the film surface, hence their expected presence on the surface, as depicted in Figure 31.

## 13.3. CONCLUSIONS ON GOLD NANOPARTICLES

- The UV-Vis analysis of the Au nanoparticle samples allowed us to observe the effect that the modification of the synthesis reaction had since having the signal at approximately 516 nm it is expected that there will be smaller particles than previously obtained with a response to wavelengths around 530 nm.

- The analysis by FESEM of the samples obtained from the Au nanoparticle synthesis, allowed to determine the size distribution, from 9 to 30 nm which allows to reach the conclusion that there is a deviation in the results of the analysis by DLS, which is why a method that only serves to estimate particle sizes.

- The analysis by UV-Vis, on the samples obtained to synthesize the Au nanoparticles, allowed to determine that the concentration of sodium citrate affects the formation of nanoparticles in a negative way, causing an increase in size.

- In the synthesis of microwave-assisted Au nanoparticles, the increase in heating cycles has a negative effect on the formation of gold nanoparticles, which translates into a low concentration and large particle size.

- The temperature distribution and the reaction time in the conventional heating synthesis (with respect to microwave-assisted synthesis) affect the

stability of the gold nanoparticles synthesized by the Turkevich method, which could be verified by microscopy analysis scanning electronics to see how there are multiple large agglomerations.

- Particle size dispersion is usually broader in microwave-assisted synthesis than by the conventional method, which can be attributed to the way it distributes heat during the reaction.

# 14. LITERATURE


[1] Chen Y, Fu K, Zhu S, Luo W, Wang Y, Li Y, et al. Reduced graphene oxide films with ultrahigh conductivity as Li-ion battery current collectors. Nano Lett 2016;16:3616–23. https://doi.org/10.1021/acs.nanolett.6b00743.

[2] Zhan X, Hu G, Wagberg T, Zhan S, Xu H, Zhou P. Electrochemical aptasensor for tetracycline using a screen-printed carbon electrode modified with an alginate film containing reduced graphene oxide and magnetite (Fe3O4) nanoparticles. Microchimica Acta 2016;183:723–9. https://doi.org/10.1007/s00604-015-1718-y.

[3] Kim H, Jang JI, Kim HH, Lee GW, Lim JA, Han JT, et al. Sheet size-induced evaporation behaviors of inkjet-printed graphene oxide for printed electronics. ACS Appl Mater Interfaces 2016;8:3193–9. https://doi.org/10.1021/acsami.5b10704.

[4] Novoselov KS, Fal'ko VI, Colombo L, Gellert PR, Schwab MG, Kim K. A roadmap for graphene. Nature 2012;490:192–200. https://doi.org/10.1038/nature11458.

[5] Tanabe I, Ryoki T, Ozaki Y. The effects of Au nanoparticle size (5-60 nm) and shape (sphere, rod, cube) over electronic states and photocatalytic activities of TiO2 studied by far- and deep-ultraviolet spectroscopy. RSC Adv 2015;5:13648–52. https://doi.org/10.1039/C4RA12503G.

[6] Yun YJ, Ju J, Lee JH, Moon S-H, Park S-J, Kim YH, et al. Highly Elastic Graphene-Based Electronics Toward Electronic Skin. Adv Funct Mater 2017;27:1701513. https://doi.org/10.1002/adfm.201701513.

[7] Jang H, Park YJ, Chen X, Das T, Kim MS, Ahn JH. Graphene-Based Flexible and Stretchable Electronics. Advanced Materials 2016;28:4184–202. https://doi.org/10.1002/adma.201504245.

[8] Kuila T, Bose S, Mishra AK, Khanra P, Kim NH, Lee JH. Chemical functionalization of graphene and its applications. Prog Mater Sci 2012;57:1061–105. https://doi.org/10.1016/j.pmatsci.2012.03.002.

[9] Li T, Li Z, Zhou J, Pan B, Xiao X, Guo Z, et al. The Application of Graphene in Biosensors. Springer, Cham 2017:299–329. https://doi.org/10.1007/978-3-319-50824-5_10.

[10] Feng C. Stretchable Graphene-based Materials of High Conductivity ACCESS TO THESIS - A 2016.

[11] Formica N, Mantilla-Perez P, Ghosh DS, Janner D, Chen TL, Huang M, et al. An indium tin oxide-free polymer solar cell on flexible glass. ACS Appl Mater Interfaces 2015;7:4541–8. https://doi.org/10.1021/am5071909.

[12] Kuo W, Hsu C, Chen H, Chang C, Kao H. Graphene quantum dots conjugated with polymers for two-photon properties under two-photon excitation. Nanoscale 2016.

[13] Wong WS, Salleo A. Flexible Electronics: Materials and Applications. vol. 1. 2009. https://doi.org/10.1007/978-0-387-74363-9.

[14] Netravali AN, Chabba S. Composites get greener. Materials Today 2003;6:22–9. https://doi.org/10.1016/S1369-7021(03)00427-9.

[15] Mohanty AK, Misra M, Drzal LT. Sustainable Bio-Composites from renewable resources: Opportunities and challenges in the green materials world. J Polym Environ 2002;10:19–26. https://doi.org/10.1023/A:1021013921916.

[16] Bismarck A, Mishra S, Lampke T. Plant fibers as reinforcement for green composites. Natural Fibers, Biopolymers and Biocomposites 2005:37–108.

[17] Bahrani M, Sharif M, Amirazodi K. Preparation and characterization of polythiophene/graphene oxide/epoxy nanocomposite coatings with advanced properties. Polymer Bulletin 2021:1–22. https://doi.org/10.1007/s00289-020-03529-1.

[18] Chen Y, Fu K, Zhu S, Luo W, Wang Y, Li Y, et al. Reduced graphene oxide films with ultrahigh conductivity as Li-ion battery current collectors. Nano Lett 2016;16:3616–23. https://doi.org/10.1021/acs.nanolett.6b00743.

[19] Zhan X, Hu G, Wagberg T, Zhan S, Xu H, Zhou P. Electrochemical aptasensor for tetracycline using a screen-printed carbon electrode modified with an alginate film containing reduced graphene oxide and magnetite (Fe3O4) nanoparticles. Microchimica Acta 2016;183:723–9. https://doi.org/10.1007/s00604-015-1718-y.

[20] Formica N, Mantilla-Perez P, Ghosh DS, Janner D, Chen TL, Huang M, et al. An indium tin oxide-free polymer solar cell on flexible glass. ACS Appl Mater Interfaces 2015;7:4541–8. https://doi.org/10.1021/am5071909.

[21] Chunfang F. Stretchable Graphene-based Materials of High Conductivity. Deakin University, 2016.

[22] Chen Y, Fu K, Zhu S, Luo W, Wang Y, Li Y, et al. Supporting Information Reduced Graphene Oxide Films with Ultra-High Conductivity as Li-ion Battery Current Collectors. 2016.

[23] Novoselov KS, Geim AK, Morozov SV, Jiang D, Zhang Y, Dubonos SV, et al. Electric field effect in atomically thin carbon films. Science (1979) 2004;306:666–9. https://doi.org/10.1126/science.1102896.

[24] Tao X, Wang X, Li Z, Zhou S. Ultralow temperature synthesis and improved adsorption performance of graphene oxide nanosheets. Appl Surf Sci 2015;324:363–8. https://doi.org/10.1016/j.apsusc.2014.10.153.

[25] McGovern IT, Holland B, Byrne M, GunKo YK, Boland JJ, Niraj P, et al. High-yield production of graphene by liquid-phase exfoliation of graphite. Nat Nanotechnol 2008;3:563568.

[26] Kim K, Zhao Y, Jang H, Lee S, Kim J, Kim K. Large-scale pattern growth of graphene films for stretchable transparent electrodes. Nature 2009.

[27] Sutter PW, Flege J-I, Sutter E a. Epitaxial graphene on ruthenium. Nat Mater 2008;7:406–11. https://doi.org/10.1038/nmat2166.

[28] Sadhukhan S, Ghosh TK, Rana D, Roy I, Bhattacharyya A, Sarkar G, et al. Studies on synthesis of reduced graphene oxide (RGO) via green route and its electrical property. Mater Res Bull 2016;79:41–51. https://doi.org/10.1016/j.materresbull.2016.02.039.

[29] Wang Y, Shi Z, Yin J. Facile Synthesis of Soluble Graphene via a Green Reduction of Graphene Oxide in Tea Solution and Its Biocomposites. ACS Appl Mater Interfaces 2011;3:1127–33. https://doi.org/10.1021/am1012613.

[30] Balandin A a, Ghosh S, Bao W, Calizo I, Teweldebrhan D, Miao F, et al. Superior Thermal Conductivity of Single-Layer Graphene 2008. Nano Lett 2008;8:902–7. https://doi.org/10.1021/nl0731872.

[31] Subrahmanyam KS, Manna AK, Pati SK, Rao CNR. A study of graphene decorated with metal nanoparticles. Chem Phys Lett 2010;497:70–5. https://doi.org/10.1016/j.cplett.2010.07.091.

[32] Eda G, Chhowalla M. Graphene-based Composite Thin Films for Electronics. Nano Lett 2009;9:814–8. https://doi.org/10.1021/nl8035367.

[33] Geetha Bai R, Muthoosamy K, Zhou M, Ashokkumar M, Huang NM, Manickam S. Sonochemical and sustainable synthesis of graphene-gold (G-Au) nanocomposites for enzymeless and selective electrochemical detection of nitric oxide. Biosens Bioelectron 2017;87:622–9. https://doi.org/10.1016/j.bios.2016.09.003.

[34] Thema F, Moloto M, Dikio E. Synthesis and characterization of graphene thin films by chemical reduction of exfoliated and intercalated graphite oxide. Journal Of 2012.

[35] Yee MSL, Khiew PS, Chiu WS, Tan YF, Kok YY, Leong CO. Green synthesis of graphene-silver nanocomposites and its application as a potent marine antifouling agent. Colloids Surf B Biointerfaces 2016;148:392–401. https://doi.org/10.1016/j.colsurfb.2016.09.011.

[36] Nguyen DD, Tai N-H, Lee S-B, Kuo W-S. Superhydrophobic and superoleophilic properties of graphene-based sponges fabricated using a facile dip coating method. Energy Environ Sci 2012;5:7908. https://doi.org/10.1039/c2ee21848h.

[37] Woltornist S. Pristine Graphene as a Two-Dimensional Surfactant. 2016.

[38] Tetlow H, Posthuma de Boer J, Ford IJ, Vvedensky DD, Coraux J, Kantorovich L. Growth of epitaxial graphene: Theory and experiment. Phys Rep 2014;542:195–295. https://doi.org/10.1016/j.physrep.2014.03.003.

[39] Abdullah-Al-Galib M, Hou B, Shahriad T, Zivanovic S, Radadia AD. Stability of few layer graphene films doped with gold (III) chloride. Appl Surf Sci 2016;366:78–84. https://doi.org/10.1016/j.apsusc.2016.01.065.

[40] Li Y, Yang J, Zhou Y, Zhao N, Zeng W, Wang W. Fabrication of gold nanoparticles/graphene oxide films with surface-enhanced Raman scattering activity by a simple electrostatic self-assembly method. Colloids Surf A Physicochem Eng Asp 2017;512:93–100. https://doi.org/10.1016/j.colsurfa.2016.10.028.

[41] Kafiah F, Khan Z, Ibrahim A, Atieh M, Laoui T. Synthesis of graphene based membranes: Effect of substrate surface properties on monolayer graphene transfer. Materials 2017;10:86. https://doi.org/10.3390/ma10010086.

[42] Peigney A, Laurent Ch, Flahaut E, Bacsa RR, Rousset A. Specific surface area of carbon nanotubes and bundles of carbon nanotubes. Carbon N Y 2001;39:507–14. https://doi.org/10.1016/S0008-6223(00)00155-X.

[43] Mohanty AK, Misra M, Hinrichsen G. Biofibres, biodegradable polymers and biocomposites: An overview. Macromol Mater Eng 2000;276–277:1–24. https://doi.org/10.1002/(SICI)1439-2054(20000301)276:1<1::AID-MAME1>3.0.CO;2-W.

[44] Bisanda ETN, Ansell MP. Properties of sisal-CNSL composites. J Mater Sci 1992;27:1690–700. https://doi.org/10.1007/BF00542934.

[45] John MJ, Thomas S. Biofibres and biocomposites. Carbohydr Polym 2008;71:343–64. https://doi.org/10.1016/j.carbpol.2007.05.040.

[46] Park BK, Jeong S, Kim D, Moon J, Lim S, Kim JS. Synthesis and size control of monodisperse copper nanoparticles by polyol method. J Colloid Interface Sci 2007;311:417–24. https://doi.org/10.1016/j.jcis.2007.03.039.

[47] Mohanty AK, Misra M, Drzal LT. Natural fibers, biopolymers, and biocomposites. CRC Press; 2005.

[48] Vilaplana F, Strömberg E, Karlsson S. Environmental and resource aspects of sustainable biocomposites. Polym Degrad Stab 2010;95:2147–61. https://doi.org/10.1016/j.polymdegradstab.2010.07.016.

[49] Soroudi A, Jakubowicz I. Recycling of bioplastics, their blends and biocomposites: A review. Eur Polym J 2013;49:2839–58. https://doi.org/10.1016/j.eurpolymj.2013.07.025.

[50] Stankovich S, Piner RD, Nguyen SBT, Ruoff RS. Synthesis and exfoliation of isocyanate-treated graphene oxide nanoplatelets. Carbon N Y 2006;44:3342–7. https://doi.org/10.1016/j.carbon.2006.06.004.

[51] Alboofetileh M, Rezaei M, Hosseini H, Abdollahi M. Effect of montmorillonite clay and biopolymer concentration on the physical and mechanical properties of alginate nanocomposite films. J Food Eng 2013;117:26–33. https://doi.org/10.1016/j.jfoodeng.2013.01.042.

[52] Nie L, Liu C, Wang J, Shuai Y, Cui X, Liu L. Effects of surface functionalized graphene oxide on the behavior of sodium alginate. Carbohydr Polym 2015;117:616–23. https://doi.org/10.1016/j.carbpol.2014.08.104.

[53] Zhang D, Chi B, Li B, Gao Z, Du Y, Guo J, et al. Fabrication of highly conductive graphene flexible circuits by 3D printing. Synth Met 2016;217:79–86. https://doi.org/10.1016/j.synthmet.2016.03.014.

[54] Singh V, Joung D, Zhai L, Das S, Khondaker SI, Seal S. Graphene based materials: Past, present and future. Prog Mater Sci 2011;56:1178–271. https://doi.org/10.1016/j.pmatsci.2011.03.003.

[55] Park S, An J, Jung I, Piner RD, An SJ, Li X, et al. Colloidal suspensions of highly reduced graphene oxide in a wide variety of organic solvents. Nano Lett 2009;9:1593–7. https://doi.org/10.1021/nl803798y.

[56] Elgrishi N, Rountree KJ, McCarthy BD, Rountree ES, Eisenhart TT, Dempsey JL. A Practical Beginner's Guide to Cyclic Voltammetry. J Chem Educ 2018;95:197–206. https://doi.org/10.1021/acs.jchemed.7b00361.

[57] VA. Application Note E-4 A Review of Techniques for Electrochemical Analysis n.d.:1–12. http://www.htds.fr/fr/files/downloads/2013/03/A-Review-of-Techniques-for-Electrochemical-Analysis.pdf.

[58] Seehra MS, Narang V, Geddam UK, Stefaniak AB. Correlation between X-ray diffraction and Raman spectra of 16 commercial graphene-based materials and their resulting classification. Carbon N Y 2017;111:380–5. https://doi.org/10.1016/j.carbon.2016.10.010.

[59] Li Y, Tang L, Li J. Preparation and electrochemical performance for methanol oxidation of pt/graphene nanocomposites. Electrochem Commun 2009;11:846–9. https://doi.org/10.1016/j.elecom.2009.02.009.

[60] Rojo F. Tablas de Espectroscopía Infrarroja 2015:1–14. http://depa.fquim.unam.mx/amyd/archivero/TablasIR_24985.pdf (accessed October 12, 2017).

[61] Ambade RB, Ambade SB, Shrestha NK, Salunkhe RR, Lee W, Bagde SS, et al. Controlled growth of polythiophene nanofibers in $TiO_2$ nanotube arrays for supercapacitor applications. J Mater Chem A Mater 2017;5:172–80. https://doi.org/10.1039/C6TA08038C.

[62] Oberhaus F V., Frense D. Catalysing electropolymerization: High-quality polythiophene films for electrochemical sensors by the utilization of fluorine

based Lewis acid catalysts. Electrochim Acta 2022;402:139536. https://doi.org/10.1016/j.electacta.2021.139536.

[63] GOTO H, OCHIAI B, MATSUMURA Y. A Direct Route to a Polybromothiophene as a Precursor for Functionalized Polythiophene by Electrooxidative Polymerization. Electrochemistry 2023:23–67008. https://doi.org/10.5796/ELECTROCHEMISTRY.23-67008.

[64] Tsai HW, Hsueh KL, Chen MH, Hong CW. Electronic and Optical Properties of Polythiophene Molecules and Derivatives. Crystals 2021, Vol 11, Page 1292 2021;11:1292. https://doi.org/10.3390/CRYST11111292.

[65] Furukawa Y, Shimokawa D. Polarons, Bipolarons, and Electrical Properties of Crystalline Conducting Polymers. Bulletin of the Chemical Society of Japan 2023;96:1243–51. https://doi.org/10.1246/bcsj.20230175.

[66] Schö Tz K, Panzer F, Sommer M, Bä H, Kö A. A spectroscopic assessment of static and dynamic disorder in a film of a polythiophene with a planarized backbone †. This Journal Is Cite This: Mater Horiz 2023;10:5538. https://doi.org/10.1039/d3mh01262j.

[67] Fanta GF, Kenar JA, Felker FC, Byars JA. Preparation of starch-stabilized silver nanoparticles from amylose–sodium palmitate inclusion complexes. Carbohydr Polym 2013;92:260–8. https://doi.org/10.1016/j.carbpol.2012.09.016.

[68] Chandra S, Kumar A, Tomar PK. Synthesis and characterization of copper nanoparticles by reducing agent. Journal of Saudi Chemical Society 2014;18:149–53. https://doi.org/10.1016/j.jscs.2011.06.009.

[69] Valdez Aguilar JÁ. Síntesis De Nanopartículas Metálicas Utilizando Bioreductores y Su Potencial Aplicación En Sensores Plasmónicos. Universidad Autónoma de Nuevo León, 2015.

[70] El-Sayed MA. Some interesting properties of metals confined in time and nanometer space of different shapes. Acc Chem Res 2001;34:257–64. https://doi.org/10.1021/ar960016n.

[71] Piella J, Basts NG, Puntes V. Size-Controlled Synthesis of Sub-10-nanometer Citrate-Stabilized Gold Nanoparticles and Related Optical Properties. Chemistry of Materials 2016;28:1066–75. https://doi.org/10.1021/acs.chemmater.5b04406.

[72] Haiss W, Thanh NTK, Aveyard J, Fernig DG. Determination of size and concentration of gold nanoparticles from UV-Vis spectra. Anal Chem 2007;79:4215–21. https://doi.org/10.1021/ac0702084.

[73] Schulz F, Homolka T, Bastús NG, Puntes V, Weller H, Vossmeyer T. Little adjustments significantly improve the Turkevich synthesis of gold nanoparticles. Langmuir 2014;30:10779–84. https://doi.org/10.1021/la503209b.

[74] Zheng T, Bott S, Huo Q. Techniques for Accurate Sizing of Gold Nanoparticles Using Dynamic Light Scattering with Particular Application to Chemical and Biological Sensing Based on Aggregate Formation. ACS Appl Mater Interfaces 2016;8:21585–94. https://doi.org/10.1021/acsami.6b06903.

[75] Khlebtsov NG. Determination of size and concentration of gold nanoparticles from extinction spectra. Anal Chem 2008;80:6620–5. https://doi.org/10.1021/ac800834n.

[76] Amendola V, Meneghetti M. Size evaluation of gold nanoparticles by UV− vis spectroscopy. The Journal of Physical Chemistry C 2009;113:4277–85. https://doi.org/10.1021/jp8082425.

[77] Haiss W, Thanh NTK, Aveyard J, Fernig DG. Determination of size and concentration of gold nanoparticles from UV-Vis spectra. Anal Chem 2007;79:4215–21. https://doi.org/10.1021/ac0702084.

[78] Daniel MC, Astruc D. Gold Nanoparticles: Assembly, Supramolecular Chemistry, Quantum-Size-Related Properties, and Applications Toward Biology, Catalysis, and Nanotechnology. Chem Rev 2004;104:293–346. https://doi.org/10.1021/cr030698+.

[79] Thanh NVK, Giang ND, Vinh LQ, Dat HT. A Low Cost Microwave Synthesis Method for Preparation of Gold Nanoparticles. Communications in Physics 2014;24:146. https://doi.org/10.15625/0868-3166/24/2/3809.

[80] Eustis S, El-Sayed MA, Rosi NL. Why gold nanoparticles are more precious than pretty gold: Noble metal surface plasmon resonance and its enhancement of the radiative and nonradiative properties of nanocrystals of different shapes. Chem Soc Rev 2006;35:209–17. https://doi.org/10.1039/B514191E.

[81] Govorov AO, Bryant GW, Zhang W, Skeini T, Lee J, Kotov NA, et al. Exciton−Plasmon Interaction and Hybrid Excitons in Semiconductor−Metal Nanoparticle Assemblies. Nano Lett 2006;6:984–94. https://doi.org/10.1021/nl0602140.

[82] Hulkoti NI, Taranath TC. Biosynthesis of nanoparticles using microbes-A review. Colloids Surf B Biointerfaces 2014;121:474–83. https://doi.org/10.1016/j.colsurfb.2014.05.027.

[83] Behzadi S, Ghasemi F, Ghalkhani M, Ashkarran AA, Akbari SM, Pakpour S, et al. Determination of nanoparticles using UV-Vis spectra. Nanoscale 2015:5134–9. https://doi.org/10.1039/C4NR00580E.

[84] Benelli G. Plant-mediated biosynthesis of nanoparticles as an emerging tool against mosquitoes of medical and veterinary importance: a review. Parasitol Res 2016;115:23–34. https://doi.org/10.1007/s00436-015-4800-9.

[85] Cao E, Lin W, Sun M, Liang W, Song Y. Exciton-plasmon coupling interactions: from principle to applications. Nanophotonics 2017;0. https://doi.org/10.1515/nanoph-2017-0059.

[86] Turkevich J, Stevenson PC, Hillier J. A STUDY OF THE NUCLEATION AND GROWTH PROCESSES I N THE SYNTHESIS OF COLLOIDAL GOLD. Discuss Faraday Soc 1951;11:55–75. https://doi.org/10.1039/DF9511100055.

[87] Turkevich J, Stevenson PC, Hillier J. The Formation of Colloidal Gold. J Phys Chem 1953;57:670–3. https://doi.org/10.1021/j150508a015.

[88] N.a. Gold Nanoparticles: Properties and Applications | Sigma-Aldrich. Sigma-Aldrich Co 2016.

[89] Her S, Jaffray DA, Allen C. Gold nanoparticles for applications in cancer radiotherapy: Mechanisms and recent advancements. Adv Drug Deliv Rev 2017;109:84–101. https://doi.org/10.1016/j.addr.2015.12.012.

[90] Abdollahi M, Alboofetileh M, Rezaei M, Behrooz R. Comparing physico-mechanical and thermal properties of alginate nanocomposite films reinforced with organic and/or inorganic nanofillers. Food Hydrocoll 2013;32:416–24. https://doi.org/10.1016/j.foodhyd.2013.02.006.

[91] Deepa B, Abraham E, Pothan LA, Cordeiro N, Faria M, Thomas S. Biodegradable nanocomposite films based on sodium alginate and

cellulose nanofibrils. Materials 2016;9:1–11. https://doi.org/10.3390/ma9010050.